ΠΑΝΕΠΙΣΤΗΜΙΟ ΚΡΗΤΗΣ - ΤΜΗΜΑ ΕΦΑΡΜΟΣΜΕΝΩΝ ΜΑΘΗΜΑΤΙΚΩΝ
Archimedes Center for Modeling, Analysis & Computation
UNIVERSITY OF CRETE - DEPARTMENT OF APPLIED MATHEMATICS
Archimedes Center for Modeling, Analysis & Computation

ACMAC's PrePrint Repository

On a selection principle for multivalued semiclassical flows

Agissilaos Athanassoulis and Theodoros Katsaounis and Irene Kyza

ON A SELECTION PRINCIPLE FOR MULTIVALUED SEMICLASSICAL FLOWS

AGISSILAOS ATHANASSOULIS, THEODOROS KATSAOUNIS, AND IRENE KYZA

ABSTRACT. We study the semiclassical behaviour of solutions of a Schrödinger equation with a scalar potential displaying a conical singularity. When a pure state interacts strongly with the singularity of the flow, there are several possible classical evolutions, and it is not known whether the semiclassical limit corresponds to one of them. Based on recent results, we propose that one of the classical evolutions captures the semiclassical dynamics; moreover, we propose a selection principle for the straightforward calculation of the regularized semiclassical asymptotics. We proceed to investigate numerically the validity of the proposed scheme, by employing a solver based on a posteriori error control for the Schrödinger equation. Thus, for the problems we study, we generate rigorous upper bounds for the error in our asymptotic approximation. For 1-dimensional problems without interference, we obtain compelling agreement between the regularized asymptotics and the full solution. In problems with interference, there is a quantum effect that seems to survive in the classical limit. We discuss the scope of applicability of the proposed regularization approach, and formulate a precise conjecture.

Keywords: *semiclassical limit for rough potential, smoothed Wigner transform, selection principle, a posteriori error control*

1. INTRODUCTION

The study of the Schrödinger equation in the semiclassical regime

$$i\hbar u_t^\hbar + \frac{\hbar^2}{2}\Delta u^\hbar - V u^\hbar = 0, \quad u^\hbar(t=0) = u_0^\hbar,$$
(1)
$$\|u_0^\hbar\|_{L^2(\mathbb{R}^d)} = 1, \qquad \hbar \ll 1$$

arises naturally in many problems of mathematical physics. A standard physical interpretation is that of the dynamics for a quantum particle, the behaviour of which is expected to resemble classical mechanics as $\hbar \to 0$, hence the term "semiclassical". Since the full solution of (1) becomes intractable for $\hbar \ll 1$, several asymptotic techniques have been developed for its approximation.

Semiclassical asymptotics can be said to be completely understood for problems with $V \in C^{1,1}(\mathbb{R}^d)$; difficulties arise for less regular potentials. In this work we will investigate some of these difficulties, and possible ways to address them.

In section 1.1 some of the main motivations for the type of problem we consider are discussed. In section 1.2 we describe the particular problem that we investigate, and in section 1.3 the main results are reported.

1.1. **Motivation and applications.** *Long distance propagation* of many wave problems can be studied as a semiclassical limit, see [18, 32]. Even for different types of equations, the difficulties caused by non-smooth coefficients are essentially similar to what we study here. A related type of problems also appear in the *homogenisation of lattices* [19, 30].

Schrödinger equations are well known to appear in the context of *paraxial approximation* to the propagation of hyperbolic waves (see e.g. [7] and references therein for examples in acoustics, as well as [24] for optics). In practical long distance problems (e.g. in geosciences and optics) the paraxial approximation is often employed, and it leads to the semiclassical Schrödinger equation. This is then used as the basis for efficient numerical and asymptotic treatment [29, 25]. Often the appearance of Lipschitz coefficients is an essential part of the modelling of the underlying physical problem [13].

Systems of the form (1) with symmetric matrix-valued potentials (smooth in x) are typically diagonalised [18]. In most regions they decouple to several scalar Schrödinger equations; in some places there exist *eigenvalue crossings*, which can be thought of as several coupled Schrödinger equations with potentials that exhibit conical singularities. This is a topic with huge literature, but still not completely understood, see e.g. [16, 23] and the references therein. The scalar Schrödinger equation with conical singularity, is thus a one-step-easier version of that problem, as pointed out in [17, 23].

One of the prime sources of eigenvalue crossing problems is *quantum molecular dynamics under the Born-Oppenheimer approximation*. In that framework, a version of (1) is formulated for the wavefunction of the nuclei. The potential V then models the nucleus-nucleus interaction (repulsive Coulomb) as well as an effective potential representing the contribution from electrons, which are taken to relax 'instantaneously' to a state defined by the position of the nuclei. The effective electronic potential then exhibits conical singularities due to electronic eigenvalue crossings. The small parameter $\hbar$ then stands for the ratio of nuclear to electronic masses, typically $10^{-3} - 10^{-4}$. For a thorough mathematical exposition of the derivation of the Born-Oppenheimer approximation see the monograph [34]; for the state of the art study of the semiclassical limit, which takes fully into account the rough potential that appears, see [3, 4].

Finally let us remark that *semiclassical limits of nonlinear Schrödinger equations* give rise to effective potentials that are non-smooth, and this can be seen as the source of many of the analytical difficulties in their study. Perhaps the nonlinear problem with the closest relation to the conical singularity is the *one-dimensional semiclassical Schrödinger-Poisson* [35]. The self-interaction potential in that case is essentially the Green's function for the Laplacian, i.e. the conical singularity $|x|$. The state of the art for the aforementioned problem, is that the Wigner measure (see section 2.1) is one of the measure-valued weak solutions for the Vlasov-Poisson, but the selection principle is not known [35]. In particular, the regularization studied here for linear problems makes sense for the Schrödinger-Poisson as well, and in principle the same approach can be employed to investigate the 1-d semiclassical Schrödinger-Poisson as well.

1.2. **Precise setting of the problem.** We will focus on problems with potentials having "conical singularities". Intuitively, these are potentials with corners. Technically, different definitions have been used for this class. In a more abstract manner, one can require that

$$(2) \qquad V(x), \partial_x V(x) \in L^1, \qquad \partial^2_{x_i x_j} V \in \mathcal{M}(\mathbb{R}^d) \ \forall i, j = 1, ..., d,$$

where $\mathcal{M}(\mathbb{R}^d)$ are the measures of bounded total variation on $\mathbb{R}^d$. A narrower definition is that there exist real valued functions $V_0, w, g \in C^\infty(\mathbb{R}^d)$ such that

$$(3) \qquad V(x) = V_0(x) + w(x)|g(x)|.$$

To fix ideas, we will work with (3).

The problem we investigate is the asymptotic treatment of the IVP (1) for $\hbar \ll 1$ with a potential satisfying (3). The precise state of the art for the problem is given by [4, 17], and discussed in section 2.3. Full interaction of the wavefunction with the singularity (the point where V fails to be smooth) is the quantum version of a particle being in "unstable equilibrium" on a non-smooth local maximum of the potential. (For a precise definition of full interaction see definition 2.1) When that happens, it is in general not possible to predict how the wavefunction, or even the coarse-scale observables (position density, current density etc) will evolve.

To take a very simple example, in the problem

$$i\hbar u_t^\hbar + \frac{\hbar^2}{2}\Delta u^\hbar + |x|u^\hbar = 0, \quad u^\hbar(t=0) = \hbar^{-\frac{1}{4}}a_0(\frac{x}{\sqrt{\hbar}}) \in L^2(\mathbb{R}),$$

it is not known how to approximate either $u^\hbar(t)$, or even $\int_{x<0} |u^\hbar(x,t)|^2 dx$ short of solving the full problem. This model problem and its extensions can be seen as simplified versions of crossing eigenvalue interactions, as well as caustics in the nonlinear Schrödinger-Poisson equation. Indeed this was the motivation for recent works on the same problem [4, 17].

In this work we extend a regularized asymptotic scheme originally introduced in [5], and we investigate whether it gives the correct asymptotics for the full interaction of pure states with the singularity. The core idea is to derive a transport equation for a macroscopic phase-space (i.e. position - momentum (x, k)) density

$\rho^\hbar(x, k, t)$, namely

$$(4) \qquad \partial_t \rho^\hbar + 2\pi k \cdot \partial_x \rho^\hbar - \frac{1}{2\pi} \partial_x V(x) \cdot \partial_k \rho^\hbar = 0, \qquad \rho^\hbar(t=0) = \rho_0^\hbar,$$

which is well-posed, easy to solve numerically, and controls the macroscopic observables of the problem in an appropriate sense. This is a modification of the well known Wigner measure approach, which is outlined in section 2. In a nutshell, a problem of the form

$$(5) \qquad \partial_t \rho^0 + 2\pi k \cdot \partial_x \rho^0 - \frac{1}{2\pi} \partial_x V(x) \cdot \partial_k \rho^0 = 0, \qquad \rho^0(t=0) = \rho_0^0,$$

is solved for the Wigner measure $\rho^0(t)$. This limit problem (5) is no longer well posed when $V \notin C^{1,1}$, hence it is necessary to seek a regularization. Thus problem (4) is a regularization of (5), with the initial datum $\rho_0^\hbar$ containing some additional $\hbar-$dependent ("quantum") information as compared to ρ_0^0. A more detailed presentation of existing phase-space methods and the scheme we propose is provided below.

At this point it is appropriate to mention a special case of full interaction with the singularity: when two wavepackets arive on the same point in phase-space, at the same time, from different trajectories, then we say we have *interference*. This can only happen on singular points of the flow, since regular bicharacteristics do not intersect each other. We note that this use of the term *interference* coincides with the one in [31]. We will have to differentiate between problems with and without interference, and as we will see there are qualitatively different behaviours in these types of problems.

1.3. **Main results.** In this paper we study the behaviour of solutions of the semiclassical Schrödinger equation when the scalar potential exhibits a conical singularity up to a timescale $T = O(1)$. There are several possible evolutions of a pure state interacting with the singularity, and a selection principle is proposed to pick one of the classical evolutions. The main idea for this regularized asymptotic scheme is the following: for some $\sigma_x, \sigma_k \in (0, 1]$ set

$$\widetilde{W}^\hbar[u](x, k) = \left(\frac{\sqrt{2}}{\sqrt{\hbar}\sigma_x}\right)^d \int_{y, x'} e^{-2\pi i k y - \frac{\hbar\pi}{2}\sigma_k^2 y^2 - \frac{2\pi}{\hbar}\frac{|x-x'|^2}{\sigma_x^2}} u(x' + \frac{y\hbar}{2})\overline{u}(x' - \frac{y\hbar}{2}) dx' dy,$$

$$\partial_t \rho^\hbar + 2\pi k \cdot \partial_x \rho^\hbar - \frac{1}{2\pi} \partial_x V(x) \cdot \partial_k \rho^\hbar = 0, \qquad \rho^\hbar(t=0) = \widetilde{W}^\hbar[u_0^\hbar].$$

Then this problem is well-posed, and it is proposed that for all $t \in [0, T]$

$$\lim_{\hbar \to 0} \langle \widetilde{W}^\hbar[u^\hbar(t)] - \rho^\hbar(t), \phi \rangle = 0 \qquad \forall \phi \text{ in an appropriate class of test-functions.}$$

This would allow the effective asymptotic approximation of the observables of $u^\hbar(t)$ through the macroscopic phase-space density $\rho^\hbar(t)$; for more details and context see section 3.1. The Hypothesis that the aforementioned scheme indeed provides a good description of the full quantum dynamics will be referred to as *Hypothesis 1* from now on.

Using a solver for the semiclassical Schrödinger equation which provides rigorous upper bounds on the error of the approximate solution [22], we investigate numerically whether Hypothesis 1 holds for concrete problems. The Schrödinger problem has very rich abstract theory (existence, uniqueness, mass and energy conservation etc), but the empirical rules of thumb, which allow the qualitative understanding of its behaviour, break down due the lack of smoothness. Here the abstract theory is exploited by the solver to investigate the qualitative behaviour conclusively. To our knowledge, this is one of the first systematic uses of a posteriori error control to investigate a qualitative evolution question for which virtually nothing is a priori known.

Mathematically speaking, one of course cannot investigate the limit as $\hbar \to 0$ by solving for particular small values of $\hbar$. However, in most practical semiclassical problems, $\hbar$ is not much smaller than 10^{-4}. Thus, investigating the validity of our scheme for $\hbar \approx 10^{-2} - 10^{-4}$ is possibly even more interesting than the limit $\hbar \to 0$. Here we work for $\hbar \in [5 \cdot 10^{-3}, 10^{-1}]$, having put the emphasis into ensuring stability and consistency in the problems that we solve, rather than pushing computations for very small values of $\hbar$. In any case the behaviour we observe seems to be quite robust, and stabilizes very quickly (more or less for $\hbar \approx 10^{-2}$).

The first result is that in the case of *non-interference*, Hypothesis 1 holds in the problems examined, and it is suggested that it should be expected to hold more generally. Moreover, non-interference should be considered to encompass the "generic interaction" with the singularity (in the sense that in general it would be improbable that two wavepackets collide exactly on the singularity).

Second, for problems *with interference*, Hypothesis 1 seems to not hold. In the problem that we examine, we see substantial discrepancy between the proposed semiclassical asymptotics and the full quantum dynamics. That said, we do observe a stable pattern emerging in interference problems – one that seems to be up to around 5% different from what Hypothesis 1 would predict.

1.4. **Structure of the paper.** In section 2 some background on semiclassical asymptotics and phase-space methods in particular is presented. With sufficient context, we then proceed to a more complete formulation of our Hypothesis in section 3, including its main qualitative implications, and why it gives rise to a well defined, practical asymptotic scheme. In section 4 we discuss the numerical methods used for the computational simulation of both the full quantum dynamics and the classical approximation. Finally in section 5 the numerical results are presented along with some processing that helps their interpretation. Conclusions and further work are discussed in section 6, and some background material is presented in Appendices A and B.

2. PHASE-SPACE METHODS FOR SEMICLASSICAL ASYMPTOTICS

2.1. **The Wigner transform.** To study the semiclassical behavior of (1), we will use the Wigner transform. For a self contained introduction, as well as the state of the art for smooth potentials, one should consult the references [26, 18]. Here the aim is to present a brief but self-contained introduction. For any $f \in L^2(\mathbb{R})$, its *Wigner transform* (WT) is defined as

$$(6) \qquad W^\hbar[f](x,k) = \int_y e^{-2\pi i k y} f(x + \frac{\hbar y}{2}) \bar{f}(x - \frac{\hbar y}{2}) dy.$$

This transform will be applied to the wavefunction $u^\hbar(t)$; we will use the shorthand notations $W^\hbar(x,k,t) = W^\hbar[u^\hbar(t)](x,k)$, $W_0^\hbar = W^\hbar[u_0^\hbar]$ when there is no danger of confusion. In principle, the WT contains the same information as the original wavefunction, but unfolded in phase space, i.e. position-momentum space $\{(x,k)\}$. It can be seen to satisfy a well-posed equation in phase-space, namely

$$(7) \qquad \partial_t W^\hbar(x,k,t) + 2\pi k \cdot \partial_x W^\hbar(x,k,t) + i \int e^{-2\pi i S y} \frac{V(x + \frac{\hbar}{2}y) - V(x - \frac{\hbar}{2}y)}{\hbar} dy \, W^\hbar(x, k-S, t) dS = 0,$$
$$W^\hbar(t=0) = W_0^\hbar.$$

The merit of the WT lies in its behavior as $\hbar \to 0$. The idea is that given a sequence of solutions of (1), $\{u^{\hbar_n}(t)\}$ with $\lim_{n \to 0} \hbar_n = 0$, then (up to extraction of a subsequence) its *Wigner measure* (WM) $W^0(t)$ is defined as an appropriate weak-$*$ limit of

$$(8) \qquad W^\hbar(t) \rightharpoonup W^0(t) \in \mathcal{M}_+^1(\mathbb{R}^{2d}),$$

where $\mathcal{M}_+^1(\mathbb{R}^{2d})$ are the probability measures on phase-space. Moreover, the WM satisfies a Liouville equation,

$$(9) \qquad \partial_t W^0(t) + 2\pi k \cdot \partial_x W^0(t) - \frac{1}{2\pi} \partial_x V \cdot \partial_k W^0(t) = 0, \qquad W^0(t=0) = W_0^0,$$

i.e. a formulation as in classical statistical mechanics. (See e.g. Théorème IV.1 of [26], Section 7.1 of [18], and Theorem A.1 in Appendix A). For smooth potentials, problem (9) can be efficiently solved, and its solution can be used to recover the macroscopic observables of the particle (e.g. position and momentum densities). The Liouville equation (9) can be solved with the method of characteristics [15]: consider the ODE for the characteristics (the classical trajectories),

$$(10) \qquad \dot{X}_{X_0,K_0}(t) = 2\pi K_{X_0,K_0}(t), \qquad \dot{K}_{X_0,K_0}(t) = -\frac{1}{2\pi} \partial_x V(X_{X_0,K_0}(t)),$$
$$X_{X_0,K_0}(0) = X_0, \qquad K_{X_0,K_0}(0) = K_0.$$

Then a classical flow ϕ_t is induced, according to

$$(11) \qquad \phi_t(x,k) = (X_{x,k}(t), K_{x,k}(t)).$$

It is straightforward to see that the solution of (9) is given by

$$W^0(t) = W_0^0 \circ \phi_{-t}.$$

At this point it is clear why the regularity of $V \in C^{1,1}(\mathbb{R}^d)$ is a natural threshold for the validity of these types of results. For $V \in C^{1,1}(\mathbb{R}^d)$, the characteristics (10) is well-defined for all $(X_0, K_0) \in \mathbb{R}^{2d}$, and thus the

WM is well defined at all times. If $V \notin C^{1,1}(\mathbb{R}^d)$, then in general the Cauchy problem (9) is not well-posed over probability measures.

In [26] it was shown that for $V \in C^1(\mathbb{R}^d)$ (under appropriate additional technical assumptions) the WM does indeed satisfy (9), which in general has multiple solutions. Thus, the WM is one of the possible classical evolutions, but it is not known which one. (A concrete example of $V \in C^1 \setminus C^{1,1}$ which gives rise to a multivalued flow is given by the saddle points $V(x) = -|x|^{1+\theta}$, $\theta \in (0,1)$). The class of potentials with conical singularities arise as another natural threshold with respect to the regularity of flows. In particular, it has been shown recently that for potentials satisfying (2), the trajectories (10) are well defined for *almost all* initial data $(X_0, K_0) \in \mathbb{R}^{2d}$. On the level of the Liouville equation, this can be seen as well-posedness with initial data in $L^1 \cap L^\infty$ [2, 9]. From a physical point of view, *almost always well-posedness* seems very attractive. Thus a natural line of investigation opens up for potentials with conical singularities: *can it be shown that the WM satisfies (9) in an appropriate sense? And if so, can (9) be meaningfully regularized to provide a well defined semiclassical approximation?*

2.2. Asymptotics and Coarse-graining.

Problem (1) gives rise to a meaningless "limit wavefunction" $u^\hbar \rightharpoonup u^0$; typically space oscillations of wavelength $O(\hbar)$ appear and are propagated by the equation leading to

$$\lim_{\hbar \to 0} u^\hbar(t) \rightharpoonup 0 \quad \text{by oscillation.}$$

So to study the semiclassical limit, one actually has to create an auxiliary problem for objects that do have meaningful limits.

A powerful and well studied asymptotic technique is based on *Coherent States* (see e.g. [12] and the references therein): assume that the initial wavefunction is of the form

$$u_0^\hbar(x) = a\left(\frac{x - q_0}{\sqrt{\hbar}}\right) e^{ip_0 \frac{x - q_0}{\hbar}};$$

under appropriate assumptions this form is then preserved by the solution of the quantum problem,

$$u^\hbar(x, t) \approx a\left(\frac{x - q(t)}{\sqrt{\hbar}}, t\right) e^{ip(t)\frac{x - q(t)}{\hbar} - i\theta(t)},$$

where all the objects $a(x, t), p(t), q(t), \theta(t)$ satisfy simple equations independent of $\hbar$ [12]. The curve $[0, T] \to \mathbb{R}^{2d} : t \mapsto (p(t), q(t))$ is the characteristic corresponding to eq. (10), thus recovering the position and momentum of the respective classical particle.

Another famous technique is *Geometrical Optics* (see e.g. [15, 33] and the references therein). This is based on another special form for the initial wavefunction, which is preserved for short times, namely the WKB ansatz,

$$u_0^\hbar(x) = A(x)e^{i\frac{S(x)}{\hbar}}.$$

This gives rise to more subtleties (in particular caustics), and continuing the solution after the caustic time is quite tedious, and depends on the exact structure of the particular problem.

Both these techniques use a particular *ansatz for the initial wavefunction* and exploit it to recover *a full representation* of the solution in the limit. While quite powerful and well developed, these are parametric methods and have the respective limitations.

The idea behind the WM is complementary: it is a non-parametric object, which captures and keeps track in time of *macroscopic* information only. Thus in general it is impossible to reconstruct a wavefunction $u^\hbar(t)$ from the corresponding WM $W^0(t)$; on the other hand the WM appears to be more flexible than a full representation. One of the most famous examples is the unfolding of caustics in phase-space, see [33] and the references therein.

To understand better the information encoded in various representations, one must consider the *quadratic observables* of the quantum state. For every operator $A^\hbar$ in an appropriate class, one can evaluate the corresponding observable

$$(12) \qquad \mathcal{A}^\hbar(t) = \langle A^\hbar u^\hbar(t), u^\hbar(t) \rangle,$$

which is interpreted as a physical measurement on the quantum particle. It was mentioned earlier that the Wigner transform "contains the same information" as the wavefunction. This can now be made precise: the

quadratic observables can also be recovered from the WT, using the Weyl calculus. In fact, an equivalent definition of the (semiclassically scaled) Weyl symbol, $A^\hbar_\mathcal{W}(x, k)$, of the operator $A^\hbar$ is that [18]

$$\langle A^\hbar u^\hbar, u^\hbar \rangle_x = \langle A^\hbar_\mathcal{W}, W^\hbar[u^\hbar] \rangle_{x,k}. \tag{13}$$

However, the WT itself is in general much more complicated to represent and process than the original wavefunction. (It is a highly oscillatory function, in twice the space dimensions, see [11, 20], Figure 15). Using the WT as an alternative to the wavefunction is not practical; as has been mentioned, its merit comes from the WM, its weak limit as $\hbar \to 0$. This is because the WM is a *coarse-grained, macroscopic* object.

To motivate this statement, it is instructive to look at coherent states: for a family of wavefunctions of the form $u^\hbar(x) = \hbar^{-\frac{d}{4}} a(\frac{x-q}{\sqrt{\hbar}}) e^{\frac{2\pi i}{\hbar} p(x-q)+i\theta}$, the corresponding WM is $W^0(x, k) = \delta(x-q)\delta(k-p)$; the shape of the envelope a is completely lost. Moreover, if $(q, p) \neq (q_1, p_1)$,

$$u^\hbar(x) = \frac{\hbar^{-\frac{d}{4}}}{2} \left[a(\frac{x-q}{\sqrt{\hbar}}) e^{\frac{2\pi i}{\hbar} p(x-q)+i\theta} + b(\frac{x-q_1}{\sqrt{\hbar}}) e^{\frac{2\pi i}{\hbar} p_1(x-q_1)+i\phi} \right] \quad \Rightarrow \tag{14}$$
$$W^0(x, k) = \delta(x-q)\delta(k-p) + \delta(x-q_1)\delta(k-p_1).$$

Both envelope shapes a, b are lost, as well as the *relative* phase of the two wavepackets, $e^{i(\phi-\theta)}$. At the same time, one can still obtain meaningful approximations of (appropriate regularity classes of) observables,

$$\langle A^\hbar u^\hbar, u^\hbar \rangle_x = \langle A^\hbar_\mathcal{W}, W^\hbar \rangle_{x,k} \approx \langle A^\hbar_\mathcal{W}, W^0 \rangle_{x,k}. \tag{15}$$

The question that arises in problems with non-smooth potentials is, *does the WM keep track of enough information to determine uniquely its evolution?* It was shown in [5] that this is not the case, at least not in the standard sense (and there exist several other problems where this is not the case; see [10]).

2.3. Conical singularities and loss of uniqueness.

It was seen that the well posedness of the ODE (10) and the Liouville equation (9) are intimately related. Let us now look at an example concerning the loss of uniqueness, namely the one-dimensional potentials

$$V^\pm(x) = \pm|x|. \tag{16}$$

For $V^+ = |x|$, the problem physically amounts to an oscillator. Although there is no strong solution of (10) once the trajectory reaches $\{x = 0\}$, by accepting weak solutions the flow is in fact well defined. Indeed, it is easy to check that the problem

$$\dot{X}(t) = 2\pi K(t), \qquad \dot{K}(t) = -\frac{1}{2\pi} sign(X(t)), \tag{17}$$
$$X(0) = 0, \qquad K(0) = K_0,$$

has a unique weak solution for all values of $K_0 \in \mathbb{R}$. (See also Figure 1). So the impact of the conical singularity here is less smoothness of trajectories, but there is no loss of uniqueness.

For $V^- = -|x|$, the problem is a singular saddle point (Figure 2). The trajectories that approach the fixed point $(x, k) = (0, 0)$ now arrive in finite time, in contrast to what happens in regular saddle points. Once they reach the fixed point, there is no unique continuation – strong or weak. Consider the characteristic starting from $(X_0, K_0) = (1, -\frac{1}{\pi\sqrt{2}})$; then each of

$$X(t) = \begin{cases} \frac{1}{2}t^2 - \sqrt{2}t + 1, & t \leqslant \sqrt{2} \\ -\frac{1}{2}(t-\sqrt{2})^2, & t > \sqrt{2} \end{cases} \qquad K(t) = \begin{cases} \frac{1}{2\pi}t - \frac{1}{\pi\sqrt{2}}, & t \leqslant \sqrt{2} \\ -\frac{1}{2\pi}(t-\sqrt{2}), & t > \sqrt{2} \end{cases} \tag{18}$$

$$\tilde{X}(t) = \begin{cases} \frac{1}{2}t^2 - \sqrt{2}t + 1, & t \leqslant \sqrt{2} \\ \frac{1}{2}(t-\sqrt{2})^2, & t > \sqrt{2} \end{cases} \qquad \tilde{K}(t) = \begin{cases} \frac{1}{2\pi}t - \frac{1}{\pi\sqrt{2}}, & t \leqslant \sqrt{2} \\ \frac{1}{2\pi}(t-\sqrt{2}), & t > \sqrt{2} \end{cases} \tag{19}$$

$$\tilde{\tilde{X}}(t) = \begin{cases} \frac{1}{2}t^2 - \sqrt{2}t + 1, & t \leqslant \sqrt{2} \\ 0, & t > \sqrt{2} \end{cases} \qquad \tilde{\tilde{K}}(t) = \begin{cases} \frac{1}{2\pi}t - \frac{1}{\pi\sqrt{2}}, & t \leqslant \sqrt{2} \\ 0, & t > \sqrt{2} \end{cases} \tag{20}$$

are weak solutions of (10) past the interaction with the singularity. In other words, a classical particle with just enough momentum to reach this saddle point, can be scattered to the right, scattered to the left, or stay
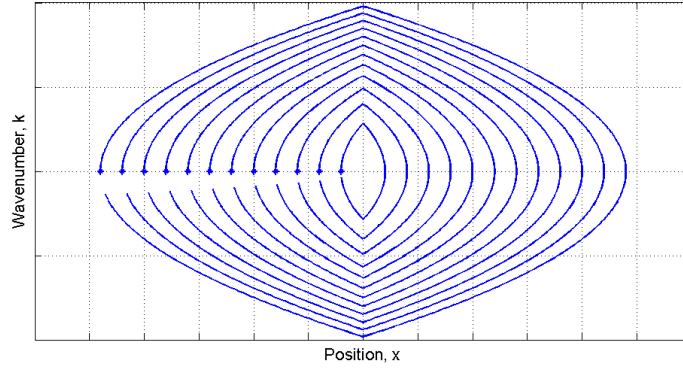
FIGURE 1. For $V = V^+$, the characteristics in phase-space can be written explicitly (in each half space $\pm X > 0$) as $X(t) = -\frac{1}{2} sign(X) t^2 + 2\pi K_0 t + X_0$, $K(t) = -\frac{1}{2\pi} sign(X) t + K_0$. Here we see plots of $(X(t), K(t))$ for $t \in [0, T]$ and various initial conditions $(X_0, 0)$. All trajectories have corners, but all are uniquely defined.
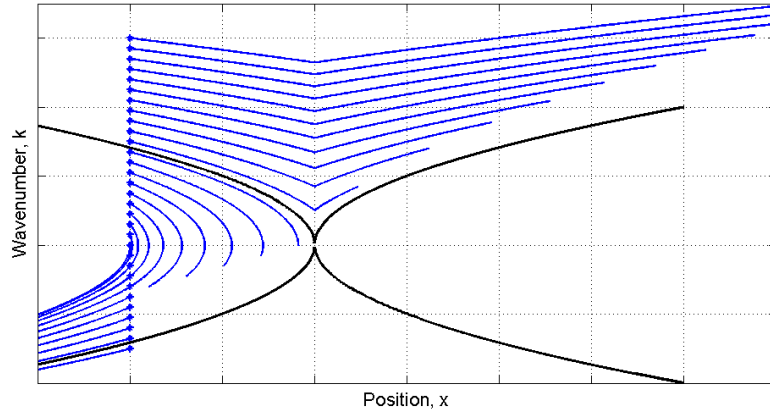

FIGURE 2. For $V = V^-$, the characteristics in phase-space can be written explicitly (in each half space $\pm X > 0$) as $X(t) = \frac{1}{2} sign(X) t^2 + 2\pi K_0 t + X_0$, $K(t) = \frac{1}{2\pi} sign(X) t + K_0$. Here we see plots of $(X(t), K(t))$ for $t \in [0, T]$ and various initial conditions $(-1, K_0)$. The separatrix $k = \pm \frac{1}{\pi} \sqrt{\frac{x}{2}}$ (shown in black) consists of two intersecting trajectories. Unlike regular saddle points, the two branches of the separatrix intersect in finite time over the fixed point $(0, 0)$.

on the saddle point indefinitely – or do combinations of the above. There are genuinely different classical evolutions to choose from here; it is not only a technical question of using the appropriate function spaces.

With respect to a more general potential of the form (3) a similar analysis has been performed in [17]. Indeed, away from the set $S = \{g(x) = 0\}$, the potential is smooth, and therefore the characteristics are well-defined and smooth. As far as the semiclassical limit is concerned, if the WM is never supported on S, then the regular theory applies [18, 17]. If however the WM arrives at some time on S, then the regular theory ceases to apply. However, the set S should really be decomposed into the disjoint union $S = S_1 \cup S_0$, where

(21)
$$\begin{aligned} S_1 &= \{g(x) = 0 \text{ and } k \cdot \partial_x g(x) \neq 0\}, \\ S_0 &= \{g(x) = 0 \text{ and } k \cdot \partial_x g(x) = 0\}. \end{aligned}$$

If a characteristic arrives at S_1, its momentum will take it "immediately" out of S, and it will be continued uniquely – with a corner. If a characteristic arrives at S_0, several classical evolutions are possible. The main result of [17] is that, as long as the WM stays away from S_0, the uniquely defined flow indeed captures correctly its evolution. This motivates the following

Definition 2.1. *A semiclassical family of problems* (1) *is said to exhibit full interaction of the wavefunction with the singularity of the flow if its WM reaches the set S_0.*

As we saw in our simple examples, to have full interaction, the initial WM W_0^0 has to be supported on a very specific (Lebesgue measure zero) subset of phase-space. It seems that a *generic* WM would *almost never* interact with S_0 and lose uniqueness. Indeed this has been made precise for non-concentrating populations of particles in [4], inspired by Born-Oppenheimer molecular dynamics. The assumptions of [4] are that the potential satisfies

$$(22) \qquad \begin{aligned} V = V_{BV} + V_C, \quad &\text{where } V_{BV} \text{ satisfies (2), and} \\ V_C &\text{ is a sum of repulsive Coulomb singularities;} \end{aligned}$$

moreover the initial data $u_0^\hbar = u_0^\hbar(\omega)$ is a stochastic population with the following property: the corresponding population of Wigner measures $W_0^0(\omega)$ is a population of delta-functions on phase-space, the centers $(X(\omega), K(\omega))$ of which have probability density function $f_0 \in L^1(\mathbb{R}^{2d}) \cap L^\infty(\mathbb{R}^{2d})$, i.e.

$$P[(X(\omega), K(\omega)) \in B \subseteq \mathbb{R}^{2d}] = \int_B f_0 \, dx \, dk, \qquad \text{for all measurable } B \subseteq \mathbb{R}^{2d}.$$

The result is that the random WMs corresponding to $u^\hbar(t; \omega)$ are delta-function the centers $(X(t; \omega), K(t; \omega))$ of which are distributed according to the solution $f(t)$ of

$$(23) \qquad \partial_t f(t) + 2\pi k \cdot \partial_x f(t) - \frac{1}{2\pi} \partial_x V \cdot \partial_k f(t) = 0, \qquad f(t = 0) = f_0.$$

Moreover, problem (23) was shown to be well posed for V as in eq. (22) and $f_0 \in L^1(\mathbb{R}^{2d}) \cap L^\infty(\mathbb{R}^{2d})$ in [4], by extending the results of [9, 2].

Certainly, in many cases this point of view is completely sufficient, and it can be said that semiclassical limits with conical singularities are "well-understood with probability 1". However, strong interactions with the singularity of the flow, and the genuine multivaluedness that it can create, is sometimes the phenomenon of interest. That is clearly reflected in the huge literature on eigenvalue crossings (which are also atypical, when considering generic random data), and of course in the Schrödinger-Poisson problem,

$$(24) \qquad i\hbar \partial_t u^\hbar + \frac{\hbar^2}{2} \Delta u^\hbar + \left(|x| * |u^\hbar|^2 \right) u^\hbar = 0, \qquad u^\hbar(t = 0) = u_0^\hbar,$$

where the convolution term carries the conical singularity around with the wavefunction, making it impossible to avoid interaction. With this in mind, we proceed to work on the possible loss of uniqueness and formulate the proposed selection principle.

3. The proposed regularization

3.1. **Formulation.** To the best of our knowledge, the state of the art for semiclassical limits with conical singularities is given by the works [17, 4]. When dealing with initial data that interact strongly with the singularity of the flow (the set S_0 of eq. (21)), there are no general rigorous results.

There exist however some partial results. In [5], the semiclassical limit of a particular class of mixed states interacting strongly with the singular saddle point $V(x) = -|x|$ was studied. Using additional information from the quantum problem, a simple selection principle was formulated. Thus for each quantum problem it is possible to choose the appropriate classical solution, which approximates it as $\hbar \to 0$. Here we will use the main idea of [5], formulate the generalization of the selection principle, and proceed to investigate numerically its validity in a more general setting.

To that end, we will need to introduce one more phase-space density. Given a problem of the form (1), let $W^\hbar(t) = W^\hbar[u^\hbar(t)]$ be the WT of the wavefunction. Denote by $\widetilde{W}^\hbar(t) = \widetilde{W}^\hbar[u^\hbar(t)]$ the corresponding

smoothed Wigner transform (SWT), defined as

$$(25) \qquad \widetilde{W}^{\hbar}(x,k) = \left(\frac{2}{\hbar \sigma_x \sigma_k}\right)^d \int\limits_{x,k} e^{-\frac{2\pi}{\hbar}\left[\frac{|x-x'|^2}{\sigma_x^2} + \frac{|k-k'|^2}{\sigma_k^2}\right]} W^{\hbar}(x',k') \, dx' \, dk'.$$

For $\sigma_x \cdot \sigma_k \geqslant 1$ it can be shown that $\widetilde{W}^{\hbar}(x,k) \geqslant 0$. Often it is useful to use smaller values for the smoothing constants, $\sigma_x, \sigma_k < 1$. In any case we will assume that the smoothing constants do not depend on $\hbar$, and are allowed to be in $\sigma_x, \sigma_k \in (0,1]$. The SWT can be thought of as a smooth, coarse-grained phase-space function. In particular, it does not contain spurious oscillations – in contrast to the WT [11, 20, 6]. In the limit the two transforms are equivalent [26],

$$\lim_{\hbar \to 0} \langle \widetilde{W}^{\hbar}(t) - W^{\hbar}(t), \phi \rangle = 0 \qquad \forall \phi \in \mathcal{A}.$$

where for the algebra of test functions $\mathcal{A}$, see Appendix A. For more context on the SWT, including on the calibration of the smoothing parameters, see Appendix B.

Now denote by $\rho^{\hbar}$ the solution of

$$(26) \qquad \begin{aligned} \partial_t \rho^{\hbar} + 2\pi k \cdot \partial_x \rho^{\hbar} - \frac{1}{2\pi} \partial_x V(x) \cdot \partial_k \rho^{\hbar} &= 0, \\ \rho^{\hbar}(t=0) &= \widetilde{W}^{\hbar}[u_0^{\hbar}]. \end{aligned}$$

Theorem 3.1. *If the potential V satisfies* (2), *then for all $\hbar > 0$ problem* (26) *is well posed in L^p for all $p \in [1, \infty]$.*

Proof: Follows by direct application of [2].

Hypothesis 1 (Proposed selection principle: the concentration limit for (26) captures the semi-classical limit for (7)). *It is proposed that for each $t \in [0, T]$*

$$(27) \qquad \lim_{\hbar \to 0} \langle \widetilde{W}^{\hbar}(t) - \rho^{\hbar}(t), \phi \rangle = 0 \qquad \forall \phi \in \mathcal{A} \cap L^2,$$

where $\rho^{\hbar}$ was defined in (26), *and the algebra of test functions $\mathcal{A}$ is defined in* (55).

Remarks:

- It is clear that if Hypothesis 1 holds, then

$$(28) \qquad \lim_{\hbar \to 0} \langle W^{\hbar}(t) - \rho^{\hbar}(t), \phi \rangle = 0 \qquad \forall \phi \in \mathcal{A} \cap L^2,$$

as well. In other words if Hypothesis 1 holds, the weak-$*$ limit of $\rho^{\hbar}$ is the Wigner measure. We state the selection principle using the SWT, because problem (26) can be considered a simpler problem to solve than (1), thus providing a meaningful asymptotic scheme. The problem

$$(29) \qquad \begin{aligned} \partial_t \rho^{\hbar} + 2\pi k \cdot \partial_x \rho^{\hbar} - \frac{1}{2\pi} \partial_x V(x) \cdot \partial_k \rho^{\hbar} &= 0, \\ \rho^{\hbar}(t=0) &= W_0^{\hbar}, \end{aligned}$$

cannot, in general, be considered a simpler problem to solve than (1) because of the spurious interference terms of the Wigner transform. Problem (29) also requires extra assumptions to ensure that $W_0^{\hbar} \in L^1$ (which is needed for well-posedness).
- It is easy to check that Hypothesis 1 is a priori consistent with the existing rigorous results [17, 4] – in addition to [5] from which it was inspired.

3.2. **Application.** Often the proposed selection principle can be used to compute $\rho^{\hbar}$ and its weak limit explicitly. This is true in particular for $d = 1$ and $V = -|x|$ (see Figure 2). For this problem, phase space $\{(x,k)\}$ can be partitioned into the disjoint union $\mathbb{R}^2 = S^+ \cup S \cup S^-$, where

$$(30) \qquad \begin{aligned} S^+ &= \{(x,k) \in \mathbb{R}^2 \mid H(x,k) = \tfrac{1}{2}(2\pi k)^2 - |x| > 0\}, \\ S^- &= \{(x,k) \in \mathbb{R}^2 \mid H(x,k) = \tfrac{1}{2}(2\pi k)^2 - |x| < 0\}, \\ S &= \{(x,k) \in \mathbb{R}^2 \mid H(x,k) = \tfrac{1}{2}(2\pi k)^2 - |x| = 0\}. \end{aligned}$$

It is clear that in the classical problem (26) mass never crosses from S^+ to S^-. Consider initial data $\widetilde{W}_0^\hbar$ that concentrate to a delta-function supported on a trajectory which reaches $(0,0)$ as $\hbar \to 0$. Then, the concentration limit of $\rho^\hbar(t)$ would split into two delta functions upon reaching $(0,0)$, moving along trajectories (18), (19) respectively, and with masses determined by $\lim_{\hbar \to 0} \int_{S^\pm} \widetilde{W}^\hbar dx dk$ (see also [5]). Indeed the amount of mass scattered to the left and the right of the singularity is a basic observable of the interaction, and among those on which the quality of the semiclassical approximation will be checked.

We will investigate numerically such problems, and examine whether the quantum dynamics agree with this classical regularization. The scenario described above is called a "non-interference problem". If the initial WM contains *two* delta functions that arrive to $(x,k) = (0,0)$ from the left and right at the same time, we say we have *interference* between the two wavepackets. (This is the concept of interference used in [31]). We will also investigate problems with interference.
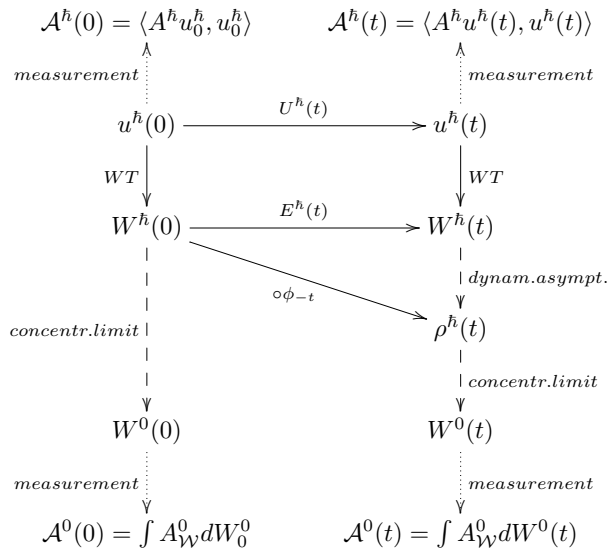
$$\mathcal{A}^\hbar(0) = \langle A^\hbar u_0^\hbar, u_0^\hbar \rangle \qquad \mathcal{A}^\hbar(t) = \langle A^\hbar u^\hbar(t), u^\hbar(t) \rangle$$

$$\begin{array}{ccc}
& \wedge & & \wedge \\
measurement & \vdots & & \vdots & measurement \\
u^\hbar(0) & \xrightarrow{\ U^\hbar(t)\ } & u^\hbar(t) \\
WT \Big\downarrow & & \Big\downarrow WT \\
W^\hbar(0) & \xrightarrow{\ E^\hbar(t)\ } & W^\hbar(t) \\
\Big| & \searrow^{\ \circ\phi_{-t}} & \Big| \ dynam.asympt. \\
concentr.limit \Big| & & \rho^\hbar(t) \\
\Big| & & \Big| \ concentr.limit \\
W^0(0) & & W^0(t) \\
measurement \vdots & & \vdots \ measurement \\
\mathcal{A}^0(0) = \int A_{\mathcal{W}}^0 dW_0^0 & & \mathcal{A}^0(t) = \int A_{\mathcal{W}}^0 dW^0(t)
\end{array}$$

FIGURE 3. The asymptotic scheme proposed in [5]: the $\hbar \to 0$ limit must now be taken in two steps: first we substitute the quantum dynamics with the classical dynamics; propagate in time, and then take the concentration limit of the Wigner transform. That way, we propagate a Liouville equation for $L^\infty \cap L^1$ data, which is well posed, and contains the quantum information needed to choose the correct weak solution. This was only proved for a narrow selection of initial data.

4. THE NUMERICAL METHOD

4.1. **Solving the semiclassical Schrödinger equation with conical singularities.** The numerical solution of (1) is complicated from the theoretical as well as from the numerical point of view. The main difficulty is that the solution of (1) oscillates with wavelength $\mathcal{O}(\hbar)$ thus standard numerical methods require very fine meshes (space and time) to resolve adequately this high oscillatory behaviour. Further the solution might exhibit caustics, making its numerical approximation even more difficult. Finally the relatively low smoothness of the potential V means that several tools widely used in the numerical analysis and simulation of such problems are now not available.

Popular methods for the numerical solution of (1) are time-splitting spectral methods and Crank-Nicolson finite element / finite difference methods. The standard Crank-Nicolson finite element / finite difference methods suffer from a very restrictive dispersive relation, cf. [21], connecting the space and time mesh sizes with the parameter $\hbar$ thus requiring considerable computational resources in order to produce accurate solutions for $\hbar \ll 1$. In an attempt to relax this restrictive dispersive relation Bao, Jin and Markowich in [8] proposed time-splitting spectral methods for the numerical solution of (1). This is widely considered to

$$\mathcal{A}^\hbar(0) = \langle A^\hbar u_0^\hbar, u_0^\hbar \rangle \qquad \mathcal{A}^\hbar(t) = \langle A^\hbar u^\hbar(t), u^\hbar(t) \rangle$$

measurement   *measurement*

$$u^\hbar(0) \Longrightarrow^{U^\hbar(t)} u^\hbar(t)$$

WT   *WT*

SWT $W^\hbar(0) \xrightarrow{E^\hbar(t)} W^\hbar(t)$

smoothing   *smoothing*   *Comparison*

$$\widetilde{W}^\hbar(0) \xrightarrow{\widetilde{E}^\hbar(t)} \widetilde{W}^\hbar(t)$$

coarse measur. $\circ\phi_{-t}$ *proposed asympt.*

$$\int A_{\mathcal{W}}^\hbar d\widetilde{W}^\hbar(0) \qquad\qquad \rho^\hbar(t) \xrightarrow{coarse\ measur.} \int A_{\mathcal{W}}^\hbar d\rho^\hbar(t)$$

concentr.lim.   *concentr.lim.*

$\hbar \to 0$ $W^0(0) \qquad\qquad W^0(t)$ $\hbar \to 0$

measurement   *measurement*

$$\mathcal{A}^0(0) = \int A_{\mathcal{W}}^0 dW_0^0 \qquad\qquad \mathcal{A}^0(t) = \int A_{\mathcal{W}}^0 dW^0(t)$$
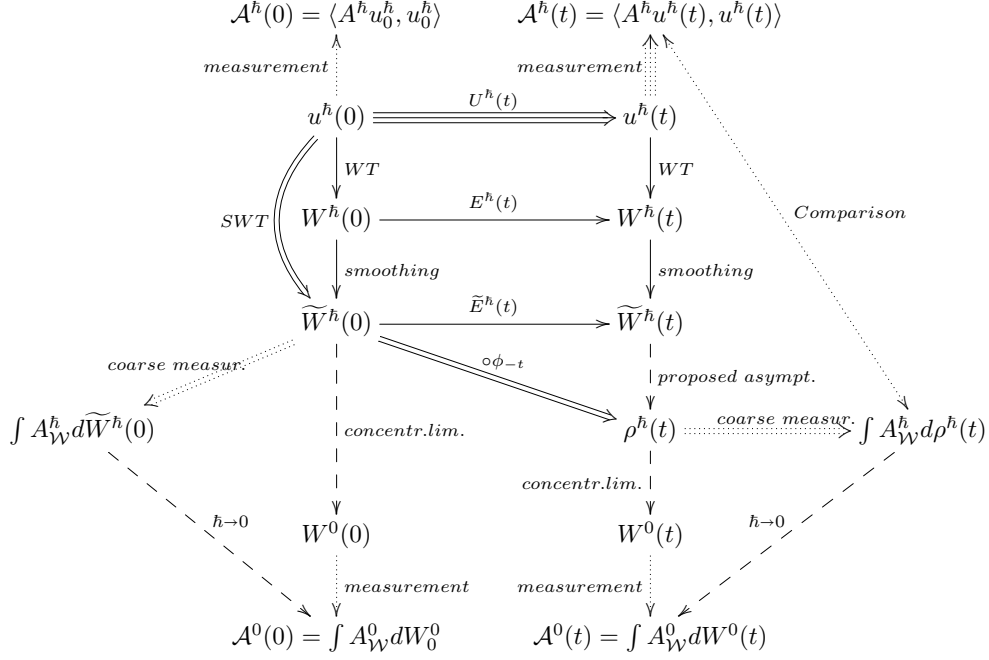
FIGURE 4. **Computational implementation of the asymptotic scheme of Figure 3: double-arrows.** One propagates a *coarse-scale* phase-space density with the Liouville equation, and not the full Wigner transform – otherwise it would be even more expensive than the direct solution of (1). Coarse-scale observables can still be accurately recovered from the smoothed density, as long as they correspond to length scales larger than the smoothing. Position densities, current flows etc typically fall in this category. This allows the investigation of the selection principle, and in fact it provides an efficient method for the computation of coarse-scale observables. **Full solution of (1): triple-arrows.**

be the preferred approach for semiclassical problems; however it requires $V \in C^2$ at least for any kind of rigorous convergence result.

A different approach to overcome this difficulty is based on adaptivity. Adaptive methods are widely used in recent years to construct accurate numerical approximations to a broad class of problems with substantially reduced computational cost by creating appropriately nonuniform meshes in space and time. There are several ways to propose an adaptive strategy. One such approach is based on rigorous a posteriori error control. The idea is to estimate the error in some natural norm by

$$\|u - U\| \le \mathcal{E}(U) \tag{31}$$

where $\mathcal{E}(U)$ a computable quantity depending on the approximate solution U and the data of the problem. A crucial property that the estimator $\mathcal{E}(U)$ must satisfy, is to converge with the same order as the numerical method. It is then said that $\mathcal{E}(U)$ decreases with optimal order with respect to the mesh discretisation parameters. The existing literature on adaptive methods based on a posteriori error bounds for the numerical approximation of (1) is very limited. Very recently the authors presented in [22], an adaptive algorithm for the numerical approximation of (1), based on a posteriori error estimates of optimal order. The proposed adaptive method proved to be competitive with the best available methods in the literature not only for the approximation of the solution of (1) but as well as for its observables, c.f. [22].

Here we want to investigate the behaviour of a quantum problem, for which we don't have even any qualitative a priori information. (E.g. the percentage of mass scattered in different directions after the interaction with the singularity). Hence a posteriori error control is particularly useful, as it provides a rigorous, quantitative grasp on the quantum interaction – making meaningful the subsequent comparison to the classical asymptotics.

4.2. **The CNFE method.** In [22] the authors consider the initial-and-boundary value problem

$$(32) \qquad \begin{cases} i\hbar u_t^\hbar + \dfrac{\hbar^2}{2}\Delta u^\hbar - V u^\hbar = f & \text{in } \Omega \times (0, T], \\[2mm] u^\hbar = 0 & \text{on } \partial\Omega \times [0, T], \\[2mm] u^\hbar(t = 0) = u_0^\hbar & \text{in } \Omega, \end{cases}$$

where $\Omega \subset \mathbb{R}^d$ is a bounded domain and $f \in L^\infty\big([0, T]; L^2(\Omega)\big)$ is a forcing term. They discretize (32) by a Crank-Nicolson finite element (CNFE) scheme and prove a posteriori error estimates of optimal order. One of the main features of the considered finite element spaces is that they are allowed to change in time. The optimal order a posteriori error bounds are derived in the $L_t^\infty L_x^2$ norm and the analysis includes time-dependent potentials. Furthermore the derived a posteriori estimates are valid for $L_t^\infty L_x^\infty$-type potentials as well, in contrast to the existing results in the literature which require smooth $C_t^1 C_x^2$-type potentials.

The analysis in [22] is based on the reconstruction technique, proposed by Akrivis, Makridakis & Nochetto, for the heat equation, cf. [1, 27]. In [22] the authors, following this technique, introduce a novel time-space reconstruction for the CNFE scheme, appropriate for the Schrödinger equation (32). A posteriori estimates for (32) and the CNFE method were also proven by Döfler in [14], but the estimator was not of optimal order in time.

The main results of [22] can be summarised as follows: The approximations $U^n(x)$ of $u^\hbar(x, t_n)$, $0 \le n \le N$, are computed for a non-uniform time grid $0 =: t_0 < t_1 < \cdots < t_N =: T$ of $[0, T]$. For each n, U^n belongs to a finite element space (which depends on n) consisting of piecewise polynomials of degree r. By $U(x, t)$ we denote the piecewise linear interpolant between the nodal values U^n. More specifically, for $t \in [t_{n-1}, t_n]$, $U(x, t) := \dfrac{t - t_{n-1}}{t_n - t_{n-1}} U^n(x) + \dfrac{t_n - t}{t_n - t_{n-1}} U^{n-1}(x)$. Then

$$(33) \qquad \|(u^\hbar - U)(t)\|_{L^2(\Omega)} \le \mathcal{E}_N^0 + \mathcal{E}_N^S + \mathcal{E}_N^T, \quad \forall t \in [0, T],$$

where $\mathcal{E}_N^0$, $\mathcal{E}_N^S$, $\mathcal{E}_N^T$ are all computable quantities. More precisely, $\mathcal{E}_N^0$ accounts for the initial error, while $\mathcal{E}_N^S$, $\mathcal{E}_N^T$ are the space and time estimators respectively. These estimators are used to refine appropriately the time and space mesh sizes, thus creating an adaptive algorithm. The algorithm is said to converge up to a preset tolerance TOL if, after appropriate refinements, we obtain an approximate solution U of u with

$$\mathcal{E}_N^0 + \mathcal{E}_N^S + \mathcal{E}_N^T < \text{TOL}.$$

In particular, in view of (33), we will then have that

$$(34) \qquad \|(u^\hbar - U)(t)\|_{L^2(\Omega)} \le \text{TOL}, \quad \forall t \in [0, T].$$

The adaptive algorithm of [22] provides efficient error control for the solution and its observables for small values of Planck's constant $\hbar$, and in particular reduces substantially the computational cost as compared to uniform meshes. It is very difficult to obtain such results via standard techniques and without adaptivity, especially when non-smooth potentials are considered. In addition, it is to be emphasized that as long as the adaptive algorithm converges, we can guarantee rigorously, based on the a posteriori error analysis, that the *total $L_t^\infty L_x^2$ error remains below a given tolerance,* TOL. For more details, see [22].

4.3. **Validation of the CNFE scheme.** We consider the one-dimensional spatial case of (32), $\Omega = (a, b)$, and we proceed to a series of numerical experiments which (a) validate the method and the estimators in (33) in terms of accuracy and (b) highlight the advantages of adaptivity. We consider the numerical solution of (32), obtained by the CNFE scheme, with initial condition

$$u_0^\hbar(x) = a_0(x) e^{i\frac{S_0(x)}{\hbar}},$$

where a_0 may or may not depend on $\hbar$. For the spatial discretisation we use finite element spaces consisting of B-splines of degree r, $r \in \mathbb{N}$. The theoretical order of convergence for the CNFE scheme is 2 in time and $r + 1$ in space; thus the expected order of convergence of the estimator $\mathcal{E}_N^S$ is $r + 1$ and of $\mathcal{E}_N^T$ is 2.

Next, our purpose is to verify numerically the aforementioned order of convergence for the estimators, for smooth and non-smooth potentials V. To this end, let $\ell \in \mathbb{N}$ count the different realisations (runs) of the experiments. We consider uniform partitions in both time and space, and let $M(\ell) + 1$ and $N(\ell) + 1$

denote the number of nodes in space (of $[a, b]$) and in time (of $[0, T]$), respectively. Then $\Delta x(\ell) := \dfrac{b-a}{M(\ell)}$ and $\Delta t(\ell) := \dfrac{T}{N(\ell)}$ denote the space and time discretisation parameters (of the ℓth realisation), respectively. The *experimental order of convergence (EOC)* s computed for the space estimator $\mathcal{E}_N^{\text{S}}$ as follows:

$$(35) \qquad \text{EOC}_{\text{S}} := \frac{\log\left(\mathcal{E}_N^{\text{S}}(\ell)/\mathcal{E}_N^{\text{S}}(\ell+1)\right)}{\log\left(M(\ell+1)/M(\ell)\right)},$$

where $\mathcal{E}_N^{\text{S}}(\ell)$ and $\mathcal{E}_N^{\text{S}}(\ell+1)$ denote the values of the space estimators in two consecutive implementations with mesh sizes $\Delta x(\ell)$ and $\Delta x(\ell+1)$, respectively. Similarly, for the time estimator $\mathcal{E}_N^{\text{T}}$ the EOC is computed as

$$(36) \qquad \text{EOC}_{\text{T}} := \frac{\log\left(\mathcal{E}_N^{\text{T}}(\ell)/\mathcal{E}_N^{\text{T}}(\ell+1)\right)}{\log\left(N(\ell+1)/N(\ell)\right)}.$$

First, let us look at a a smooth double well potential problem with initial data

$$(37) \quad V(x) = (x^2 - 0.25)^2, \quad a_0(x) = \mathrm{e}^{-\frac{25}{2}x^2}, \quad S_0(x) = -\frac{1}{5}\ln\left(\mathrm{e}^{5(x-0.5)} + \mathrm{e}^{-5(x-0.5)}\right), \quad \text{with } \hbar = 0.25.$$

The computational domain is $[a, b] \times [0, T] = [-2, 2] \times [0, 1]$. For the double well potential (37) we use cubic

(A) Space Estimator

M	$\mathcal{E}_N^{\text{S}}$	EOC$_{\text{S}}$
35	7.4125e−01	–
50	1.6791e−01	4.1633
70	4.1761e−02	4.1354
100	9.7450e−03	4.0799
145	2.1714e−03	4.0407
200	5.9598e−04	4.0205

(B) Time Estimator

N	$\mathcal{E}_N^{\text{T}}$	EOC$_{\text{T}}$
80	1.7266e−02	–
160	3.9316e−03	2.1347
320	9.6275e−04	2.0299
640	2.3943e−04	2.0076
1280	5.9784e−05	2.0018
2560	1.4942e−05	2.0003

TABLE 1. EOC$_{\text{S}}$ and EOC$_{\text{T}}$ for Double Well potential

B-splines for the spatial discretization. The results are shown in Table 1. The predicted theoretical order of convergence is observed for both the space and time estimators.

Now let us look at a problem with a non-smooth potential, namely

$$(38) \qquad V(x) = 10|x|, \quad a_0(x) = \hbar^{-\frac{1}{4}}\mathrm{e}^{-\frac{\pi}{2\hbar}(x-x_0)^2}, \quad S_0(x) = 25\sqrt{1.5}(x - x_0), \quad \text{with } \hbar = 0.5.$$

We use quartic B-spline for the space discretisation and $[a, b] \times [0, T] = [-4, 4] \times [0, 0.1]$ is the computational domain. The numerical results are shown in Table 2 demonstrating the correct order of convergence for the estimators. It is worth noting that in this case the wavepacket passes over the non-smooth point $x = 0$ during the simulation time.

(A) Space Estimator

M	$\mathcal{E}_N^{\text{S}}$	EOC$_{\text{S}}$
800	1.4268e−01	–
1000	4.5514e−02	5.1204
1200	1.8094e−02	5.0594
1600	4.3186e−03	4.9799
2000	1.4135e−03	5.0051
3200	1.3481e−04	4.9998

(B) Time Estimator

$\Delta t \times 10^6$	$\mathcal{E}_N^{\text{T}}$	EOC$_{\text{T}}$
10	1.5731e−03	–
5.724	5.1538e−04	2.0001
3.629	2.0715e−04	2.0001
1.768	4.9168e−05	1.9999
1.012	1.6109e−05	2.0000
0.312	1.5312e−06	1.9999

TABLE 2. EOC$_{\text{S}}$ and EOC$_{\text{T}}$ for non-smooth potential

Finally, to observe the benefits of adaptivity, we consider a time dependent potential, namely

$$
(39) \qquad V(x,t) = \frac{x^2}{2(t+0.05)}, \quad a_0(x) = \mathrm{e}^{-\lambda^2(x-0.5)^2}, \quad S_0(x) = 5(x^2 - x) \quad \text{with } \hbar = 1.
$$

The computational domain is $[a,b] \times [0,T] = [-1,2] \times [0,1]$ and we discretize space using cubic B-splines. In Figure 5, we plot the evolution of the estimators in logarithmic scale and the variation in time of the time-steps $\Delta t_n := t_n - t_{n-1}$ and of the degrees of freedom. This is a characteristic example where intensive adaptivity is observed, in both time and space.
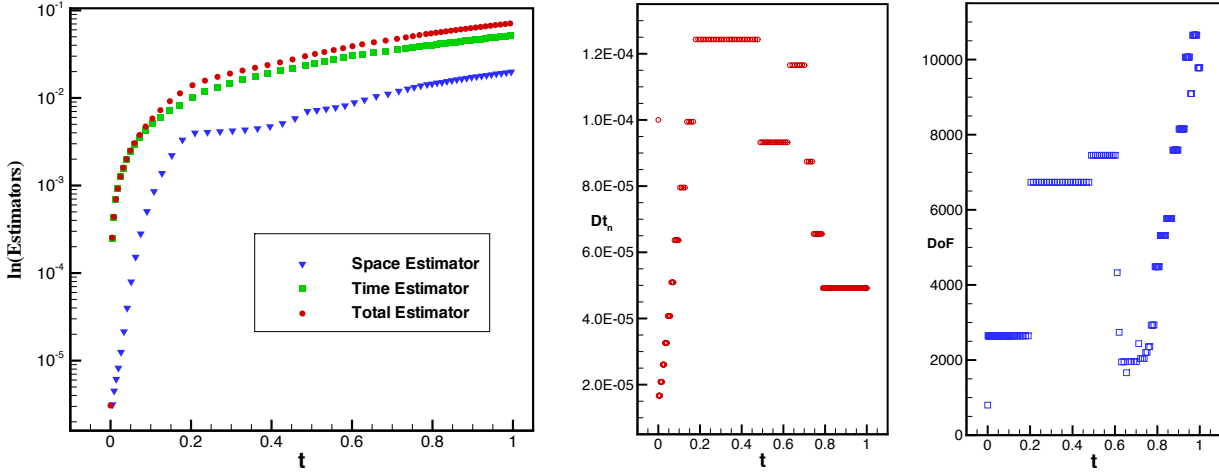
FIGURE 5. Evolution of estimators in logarithmic scale (left) and variation of the time-steps Δt_n and the degrees of freedom (DoF) versus t (right) during adaptivity for $V(x,t) = \dfrac{x^2}{2} \cdot \dfrac{1}{t+0.05}$.

4.4. **Approximation of the observables of problem** (1). As always when discretizing problems in free space, we have to make sure the interval $[a,b]$ is large enough so that (for the initial data $u_0^\hbar$ and timescale T in question) the solutions of problems (32), (1) are close to each other. This follows from standard localization arguments, and it is easy to check it in practice (by measuring how much mass reaches the endpoints) and poses no particular difficulty here. Hence eq. (34) can be interpreted as an approximation between the numerical solution U and the exact solution of the free space problem (1). Here we discuss systematically how this bound can be used for the approximation of quadratic observables of the wavefunction $u^\hbar(t)$.

The quadratic observable with symbol $A(x,k)$ is defined as

$$
\mathcal{A}\Big(u^\hbar(t)\Big) = \langle\, W^\hbar[u^\hbar] \,,\, A \,\rangle = \int e^{-2\pi i K(X+Y)} A\left(\tfrac{X+Y}{2}, \hbar K\right) dK \; u^\hbar(X) dX \; \overline{u^\hbar}(Y) dY.
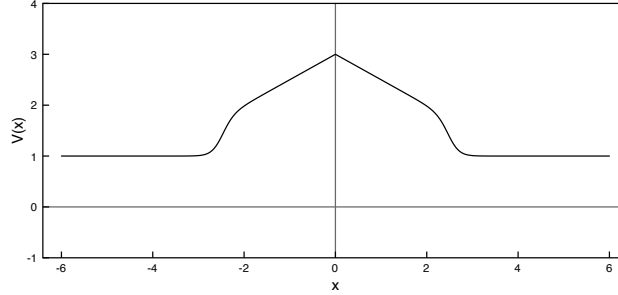$$

We will be concerned with two special types of observables, namely *observables of position*, for $A = A(x)$

$$
(40) \qquad \mathcal{A}\Big(u^\hbar(t)\Big) = \langle\, W^\hbar[u^\hbar] \,,\, A \,\rangle = \int A(x) u^\hbar(x,t) \overline{u^\hbar(x,t)} dx,
$$

and *separable observables*, $A = A_1(x) A_2(k)$,

$$
(41) \qquad \langle\, W^\hbar[u^\hbar] \,,\, A \,\rangle = \hbar^{-1} \int e^{-2\pi i K \frac{(X+Y)}{\hbar}} A_2(K) \, dK \quad A_1\left(\tfrac{X+Y}{2}\right) \quad u^\hbar(X) dX \quad \overline{u^\hbar}(Y) dY.
$$

These observables are essentially controlled by the $L_t^\infty L_x^2$ norm of the wavefunction; this is made more precise in the following

FIGURE 6. The non-smooth potential V of eq. (44).

Lemma 4.1 (Approximation of observables)**.** *If $\|u - U\|_{L^2} \leqslant$ TOL as in (34), then for every observable of position*

$$|\mathcal{A}(u) - \mathcal{A}(U)| \leqslant \text{TOL}(\|U\|_{L^2} + \|u\|_{L^2})\|A\|_{L^\infty} = O(\text{TOL}), \tag{42}$$

while for any separable observable

$$|\mathcal{A}(u) - \mathcal{A}(U)| \leqslant \hbar^{-\frac{1}{2}}\text{TOL}(\|U\|_{L^2} + \|u\|_{L^2})\|A\|_{L^2} = O(\hbar^{-\frac{1}{2}}\text{TOL}). \tag{43}$$

The proof follows by inspection of eqs. (40), (41).

Remark: The estimate (43) is far from sharp (in fact for regular, localized observables the $\hbar^{-\frac{1}{2}}$ is very pessimistic. Still, carrying out rigorously a sharper microlocal estimate for a non-smooth problem is outside the scope of this work. We note that, even with a problematic constant, it is seen rigorously that the L^2 approximation of the wavefunction does control the observables). Thus by having control over L^2 errors, we can guarantee the reliable control of L^2 observables as well.

4.5. **Particles for the Liouville equation.** To approximate numerically the solution of (26), we use a particle method; decompose the initial condition

$$\widetilde{W}_0^\hbar \approx \sum_{j=1}^N M_j \delta(x - X_j, k - K_j);$$

then the center of each particle moves along its respective trajectory, in accordance to (10). (See also the caption of Figure 2 for an explicit form of the trajectories). Thus

$$\widetilde{W}^\hbar(t) \approx P^\hbar(t) = \sum_{j=1}^N M_j \delta(x - X_j(t), k - K_j(t)).$$

The advantage in this case is that we know explicitly the trajectories, and therefore

$$\langle \widetilde{W}^\hbar(t) - P^\hbar(t), \phi \rangle = \langle \widetilde{W}_0^\hbar - P^\hbar(0), \phi \rangle \quad \forall \phi \in \mathcal{A}.$$

This makes it easy to generate approximations of observables of $\rho^\hbar(t)$ (i.e. $\int \rho^\hbar(x,k,t)A(x,k)dxdk \approx \sum_j M_j A(X_j(t), K_j(t))$) with predetermined accuracy.

5. NUMERICAL RESULTS

In this section we present a series of one-dimensional numerical experiments with the non-smooth potential of type (3)

$$V(x) = 1 + (1 + \tanh(4(x + 2.5)))(1 + \tanh(-4(x - 2.5)))\frac{(-|x| + 4)}{8}. \tag{44}$$

This potential incorporates the non-smoothness at $x = 0$ with a smooth transition to a constant state away from it. Note that in a neighbourhood of $x = 0$, V is very close to $-\frac{|x|}{2} + 3$. We use TOL ≈ 0.01 (more specifically TOL $\in [0.005, 0.02]$) in the numerical results that follow.

5.1. **Non-interference.** For values of $\hbar$ ranging from $5 \cdot 10^{-1}$ to $5 \cdot 10^{-3}$, we simulate the evolution in time of wavepackets of the form

$$(45) \qquad u_0(x) = a_0(x)e^{im\frac{S_0(x)}{\hbar}}, \quad a_0(x) = \hbar^{-\frac{1}{4}}e^{-\frac{\pi}{2}(\frac{x-x_0}{\sqrt{\hbar}})^2}, \quad S_0(x) = \sqrt{|x_0|}(x - x_0),$$

for $x_0 = -1.5$, $m \in [0.8165, 1.4289]$.

When $m = 1$, the SWT $\widetilde{W}^\hbar[u^\hbar]$ of this problem is centered on $(-1.5, \sqrt{\frac{3}{2}})$; this point reaches zero in $t = \sqrt{6}$, and roughly half the mass of the quantum particle – should (27) hold – is expected to pass to $\{x > 0\}$, while the other half should reach close to $x = 0$ and then be reflected back to $\{x < 0\}$. By perturbing the value of m in the initial data, the amount of mass expected to cross over to $\{x > 0\}$ changes (from no mass crossing over, to all the mass crossing over in the extreme cases). In all of these case studies the interaction with the singularity starts around $t = 1.3$ and is over around $t = 2.45$. (Thus e.g. before the interaction with $x = 0$ the classical and quantum solutions should agree very closely – this provides one more opportunity to validate and check our computations). We estimate how well (27) is satisfied by looking at approximations of the SWT in phase space, as well as the observables with symbols

$$(46) \qquad A_{\alpha,\beta,j}(x, k) = x^\alpha \, k^\beta \, \chi_{[0,4]}((-1)^j x)\chi_{[-1,1]}(k), \qquad \text{for } \alpha, \beta \in \mathbb{N}_0, \ \alpha + \beta \leqslant 2, \ j \in \{1, 2\}.$$

The precise measurement of these observables corresponds to

$$\langle \, W^\hbar \, , \, x^\alpha k^\beta \, \chi_{[0,4]}((-1)^j x)\chi_{[-1,1]}(k) \, \rangle =$$

$$= \int e^{-2\pi i K(X+Y)} \left[\chi_{[0,4]}((-1)^j \frac{X+Y}{2})\chi_{[-1,1]}(\hbar K)(\frac{X+Y}{2})^\alpha (\hbar K)^\beta \right] dK \quad u^\hbar(X) \, dX \quad \overline{u^\hbar}(Y) \, dY.$$

For $\beta = 0$ these are observables of position only, so by the estimate (42) we have a very good approximation. For $\beta > 0$ we do not attempt to saturate the estimate (43), since it is quite clear from the numerical results that it is not necessary. Our findings are fully consistent for both types of observables, as we will see below. The coarse-grained measurement for the same observables is

$$(47) \qquad \langle \widetilde{W}^\hbar, x^\alpha k^\beta \, \chi_{[0,4]}((-1)^j x)\chi_{[-1,1]}(k)\rangle,$$

for the quantum problem, and

$$(48) \qquad \langle \rho^\hbar, x^\alpha k^\beta \, \chi_{[0,4]}((-1)^j x)\chi_{[-1,1]}(k)\rangle,$$

for the proposed semiclassical problem. Because the observables themselves do not have any fine scales, the fine and coarse measurements are very close.

The agreement we find between the quantum dynamics and the proposed semiclassical asymptotics is striking already from relatively large values of $\hbar$. This is not entirely unexpected, as away from $x = 0$ the Liouville equation (9) is in fact identical with the full quantum dynamics (7). The finding is that "nothing non-classical happens" on $x = 0$ either, as can be clearly seen in Figures 7, 8 and 10.

Qualitatively this behaviour also appeared in investigating problems with different envelopes and other values of $\hbar$. This creates a compelling sense that in non-interference problems, the classical asymptotics – regularized through (26) – are valid. In Appendix C an even more singular example can be seen to be correctly captured by the regularized semiclassical asymptotics.

5.2. **Collision of two wave packets.** Since this is an one-dimensional problem, the only way to have interference is by one wavepacket arriving to $x = 0$ from the left, and one from the right at the same time. So we consider the collision of two wave packets, symmetrically located around $x = 0$, traveling with same velocities and opposite directions. The two wavepackets have a phase difference of an angle $2\pi\theta$, $0 \leq \theta \leq 1$. They meet at the corner point of the potential, they interact and continue to travel in opposite directions until they are completely separated. We vary the parameter θ and we study its effect on the amount of *mass* located to each side of the corner after the crossing is completed. The computational domain is taken
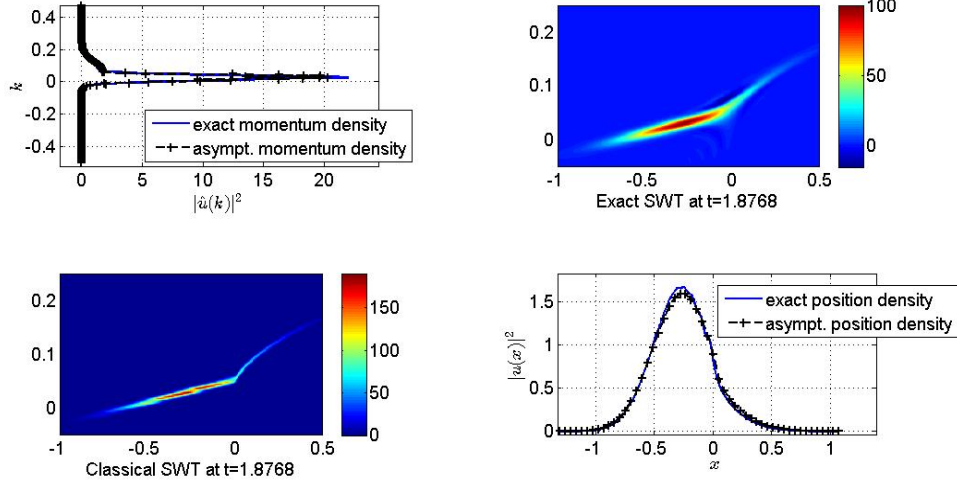
FIGURE 7. Numerical result for $\hbar = 10^{-2}$, $m = 0.9186$. Top right: Exact SWT. Top left: momentum density (dx integral of SWT). Bottom right: position density (dk integral of the SWT). Bottom left: $\rho^{\hbar}(t)$. (Note that in the SWT plots the wavenumber is scaled with $\frac{1}{2\pi}$).
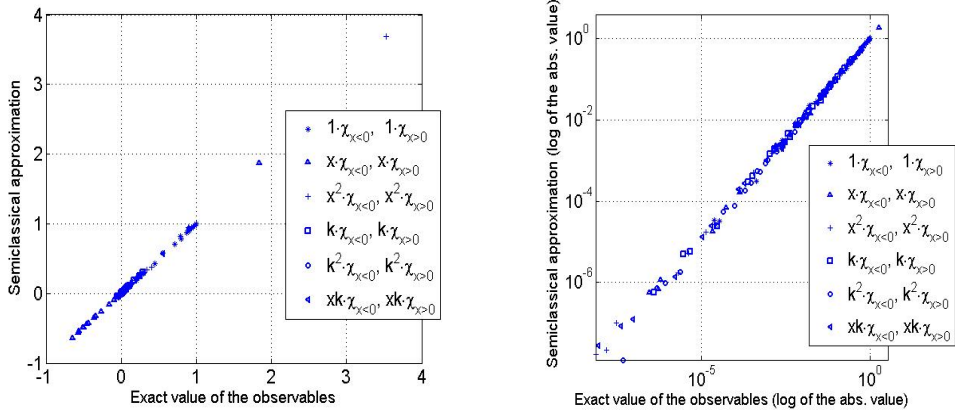

FIGURE 8. Observable measurements, for the observables in (46) and $\hbar = 10^{-2}$, $m \in \{0.8165, 0.8777, 0.9186, 1.0206, 1.4289\}$, at times $t \in [1.1788, 2.3577]$. The x−coordinate of each point is the measurement on the numerical solution $U(t)$, $\mathcal{A}_{quant} = \langle A(x,k), W^{\hbar}[U(t)] \rangle$, and the y−coordinate is the corresponding classical measurement $\mathcal{A}_{cl} = \langle A(x,k), P^{\hbar}(t) \rangle$. Note that the times used here roughly span the interaction time, in which any discrepancy between the classical and quantum dynamics could occur. More specifically the interaction starts around $t = 1$ and is over by $t = 2.4$ for all the problems.

sufficiently large to avoid possible interactions with the boundary and we discretise in space using quintic B-splines. The initial condition is of the form

$$(49) \quad \begin{aligned} u_0(x) &= a_{0,1}(x)\mathrm{e}^{i\frac{S_{0,1}(x)}{\hbar}} + a_{0,2}(x)\mathrm{e}^{i\frac{S_{0,2}(x)}{\hbar}}\mathrm{e}^{i2\pi\theta}, \quad 0 \le \theta \le 1, \\ a_{0,1}(x) &= \hbar^{-\frac{1}{4}}\mathrm{e}^{-\frac{\pi}{2}\left(\frac{x-x_0}{\sqrt{\hbar}}\right)^2}, \quad a_{0,2} = \hbar^{-\frac{1}{4}}\mathrm{e}^{-\frac{\pi}{2}\left(\frac{x+x_0}{\sqrt{\hbar}}\right)^2}, \\ S_{0,1}(x) &= \sqrt{|x_0|}(x-x_0), \quad S_{0,2}(x) = -\sqrt{|x_0|}(x+x_0). \end{aligned}$$
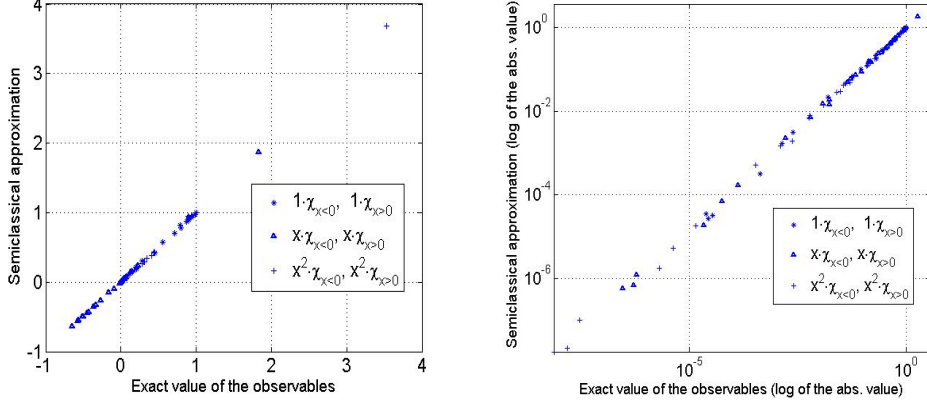
FIGURE 9. Measurements of observables of position only. The qualitative behaviour is consistent with the larger dataset. These benefit from better accuracy, by virtue of eq. (42). It is clear that qualitatively the picture doesn't change when we include observables depending on momentum as well (i.e. as in Figure 8). This is not surprising, since the simple estimate of eq. (43) is known to be pessimistic.
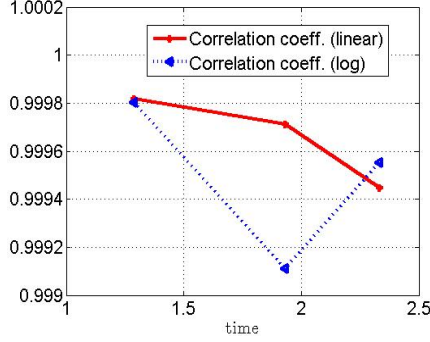

FIGURE 10. Given two vectors of measurements $\vec{x}$ and $\vec{y}$, where we expect $x_i \approx y_i$, a standard way to measure how well they line up is through the correlation coefficient $\rho_{x,y} = \frac{\langle \vec{x}, \vec{y} \rangle}{\|\vec{x}\| \, \|\vec{y}\|}$, with $\rho_{x,y} = 1$ if the two vectors are exactly aligned. Here we plot the correlation coefficients for groupings of measurements that correspond to early, high and late interaction stages. We use both the linear and log scaling (as in Figure 8). The agreement is striking (and most probably numerical errors are comparable to any quantum-classical discrepancies).

In Figure 11 the graphs of $u_0(x)$, $|u_0(x)|^2$ are shown for $\hbar = 10^{-2}$. The wave packets are located initially at $x_0 = -\frac{3}{2}$ and $-x_0 = \frac{3}{2}$ respectively. The initial step of the adaptive algorithm resolves correctly the profile of u_0 producing an initial mesh, depicted also in Figure 11, of around 1000 points with an initial error bound approximately 10^{-9}. In what follows the total error (33) is kept under 10^{-2}. In Figure 13 the mass distribution is shown for three values of the parameter $\theta = \frac{1}{4}, \frac{1}{2}, \frac{3}{4}$ and two values of Planck's constant 10^{-2}, $5 \cdot 10^{-3}$. The snapshots correspond to a time where the two wave packets have interacted with each other over the corner of the potential and continue to move away from it. In Figure 12 we see the numerical approximations for $\widetilde{W}^{\hbar}[u^{\hbar}]$ and $\rho^{\hbar}$ at a time after the interaction. The classical approximation is completely symmetric, while the quantum result is not. This is a case of a "microscopic" (i.e. invisible in the WM of the problem) feature, the phase-difference θ, playing a non-negligible "macroscopic" role.
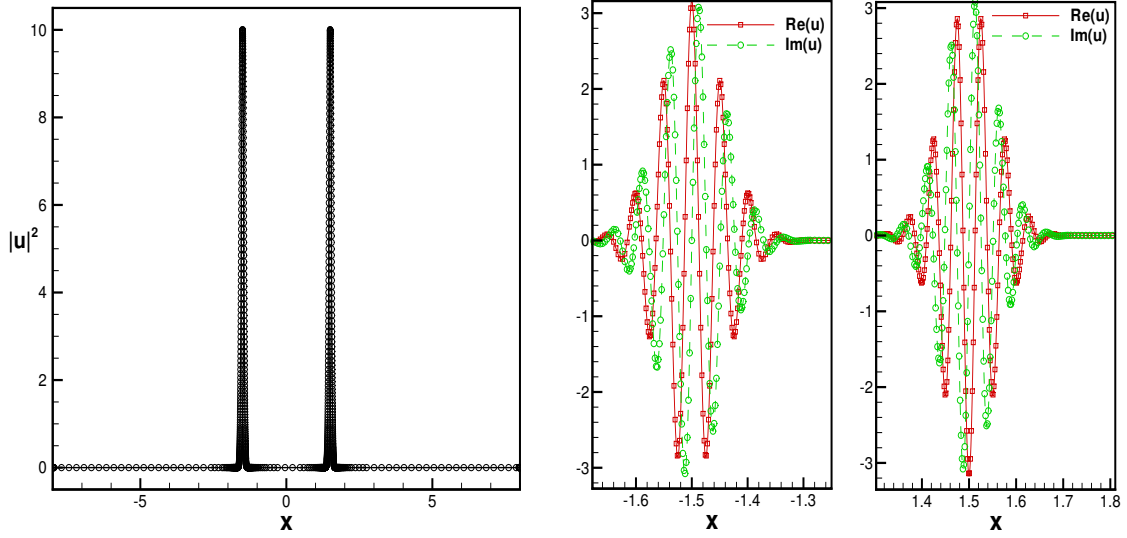
FIGURE 11. Visualization of u_0 (as defined in (49), for $\hbar = 1e - 2$). Left: Position density. Right: Real and imaginary parts for the two components of u_0 (right)
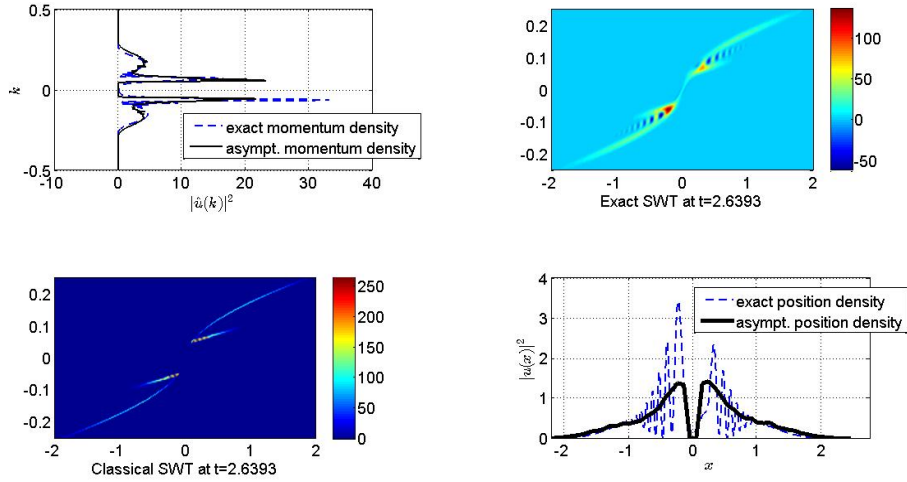

FIGURE 12. Numerical result for $\hbar = 5 \cdot 10^{-3}$, $\theta = \frac{18}{24}$. Top right: Exact SWT. Top left: momentum density (dx integral of SWT). Bottom right: position density (dk integral of the SWT). Bottom left: $\rho^\hbar(t)$. (Note that in the SWT plots the wavenumber is scaled with $\frac{1}{2\pi}$).

This non-symmetry of the mass distribution depends on the phase separation of the two wave packets and on the value of $\hbar$. Since mass is conserved – analytically as well as numerically – the excess mass in one side is compensated by less mass on the other side of the corner. We measure this by the excess mass percentage (EMP) after the interaction,

$$EMP = \|U(t_*)\chi_{x>0}\|_{L^2}^2 - \|U(t_*)\chi_{x<0}\|_{L^2}^2 \in [-1, 1]$$

(for time $t_* > 2.5$ so that the interaction is complete, and the two waves travel away from $x = 0$ in opposite directions).
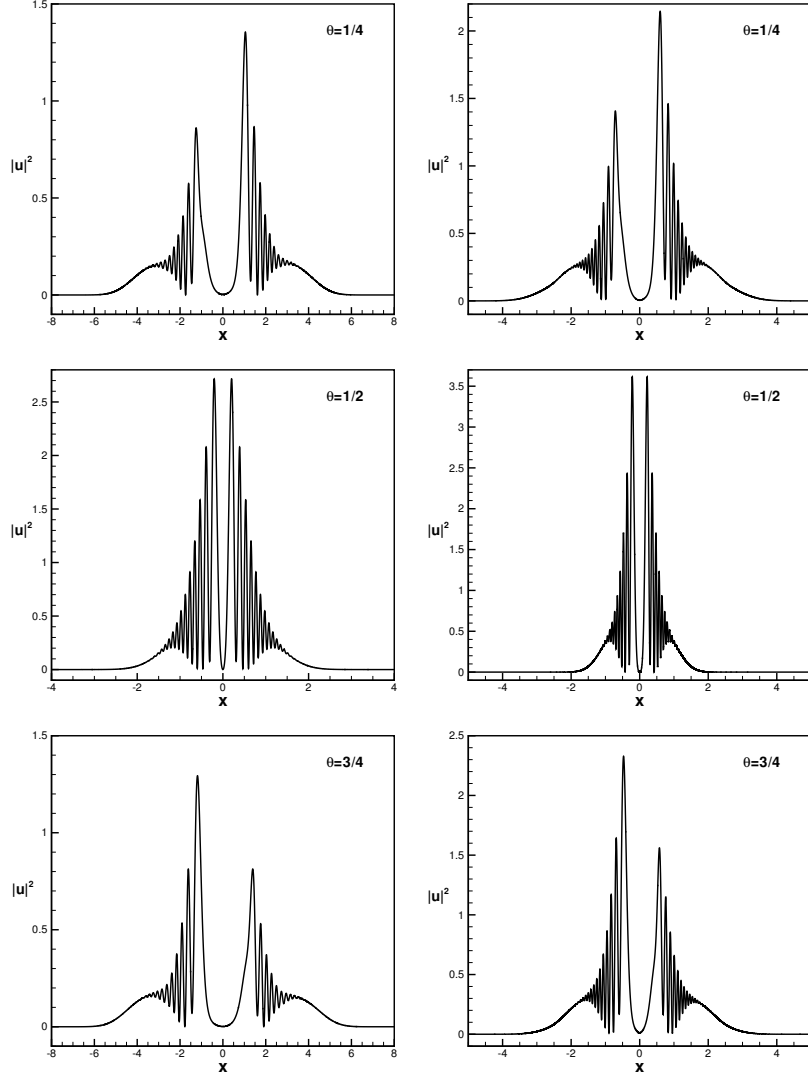
FIGURE 13. Mass distribution of (49) after the interaction for various values of θ: $\hbar = 10^{-2}$(left) and $\hbar = 5 \cdot 10^{-3}$(right)

For $\theta = \frac{1}{4}$ the wave packets have a $\frac{\pi}{2}$ phase difference and more mass, is located to the right of the corner, EMP $\approx 5\%$. In a completely analogous way for a phase separation of $\frac{3\pi}{2}$ $(\theta = \frac{3}{4})$ the exactly same amount of excess mass is shifted to the left of the corner. However for $\theta = 0, \frac{1}{2}, 1$ the mass is distributed equally around the corner, EMP $= 0$.

The dependance of the mass imbalance on Planck's constant $\hbar$ is not easily visible from Figure 13. To clarify the situation we run several numerical experiments for a variety of values of $\hbar$ and θ :

$$\theta = (2, 3, 4, 6, 8, 9, 12, 14, 17, 18, 21, 23)/24,$$
$$\hbar = 5 \cdot 10^{-1}, 10^{-1}, 5 \cdot 10^{-2}, 10^{-2}, 5 \cdot 10^{-3}.$$

The results are summarised in Figure 14 where the variation of the EMP to the right of the corner $x = 0$ is shown. The dependence on the value of $\hbar$ is evident. The location of maximum and minimum values of EMP depend solely on the value of θ and occurs for $\theta = \frac{1}{4}$ and $\theta = \frac{3}{4}$ respectively but does not depend on $\hbar$. The value of this maximum and minimum depend on the value of $\hbar$, and seem to stabilize for $\hbar$ small enough.

For $\hbar = \mathcal{O}(1)$, EMP $\approx 12.5\%$, and it reaches an apparent limiting value of EMP $\approx 5.5\%$ for $\hbar = 5 \cdot 10^{-3}$. We also notice for $\theta = 0, \frac{1}{2}, 1$ and for any value of $\hbar$ the mass is distributed evenly around the corner, EMP $= 0$. The behaviour encoded in Figure 14 seems to persist even if change the envelopes $a_{0,1}$, $a_{0,2}$; i.e. there seems to be a quantum scattering operator that depends only on the phase difference of the interfering waves.

In these problems, for all $\theta, \hbar$, the classical model (26) yields EMP ≈ 0. Here the smoothing introduced in the initial data is not entirely innocent, and in fact the solution of (29) yields a different result. This is to be expected, because

$$W^{\hbar}[u_0^{\hbar}](x,k) = \frac{2}{\hbar} e^{-\pi \frac{(x-x_0)^2}{\hbar} - 4\pi \frac{(k-\frac{\sqrt{|x_0|}}{2\pi})^2}{\hbar}} + \frac{2}{\hbar} e^{-\pi \frac{(x+x_0)^2}{\hbar} - 4\pi \frac{(k+\frac{\sqrt{|x_0|}}{2\pi})^2}{\hbar}}$$
$$+ 2Re\left(\frac{2}{\hbar} e^{-\frac{\pi}{\hbar} x^2 - \frac{4\pi}{\hbar} k^2} e^{-2\pi i\theta - \frac{2i\sqrt{|x_0|}}{\hbar} x + 4\pi i x_0 k}\right).$$

The third term is suppressed by the smoothing (since it is highly oscillatory), but being supported over zero it does affect the mass balance. Still, the EMP for eq. (29) does not seem to agree with that of the quantum problem, but a more systematic investigation of that question is needed. In any case, eq. (29) cannot be considered a semiclassical asymptotic scheme; investigating its behaviour can in fact be harder than solving the full quantum problem.

The discrepancies between the scheme of eq. (26) due to this quantum mass exchange seem to be at most $\pm 5\%$ for small values of $\hbar$; and in fact other observables fare somewhat better. So although we can report that (26) does not provide the correct solution for interference problems, it does give a meaningful qualitative picture of what takes place, plus or minus some mass exchange. Depending on the context, it could conceivably provide a viable approximation, or a starting point for perturbation.
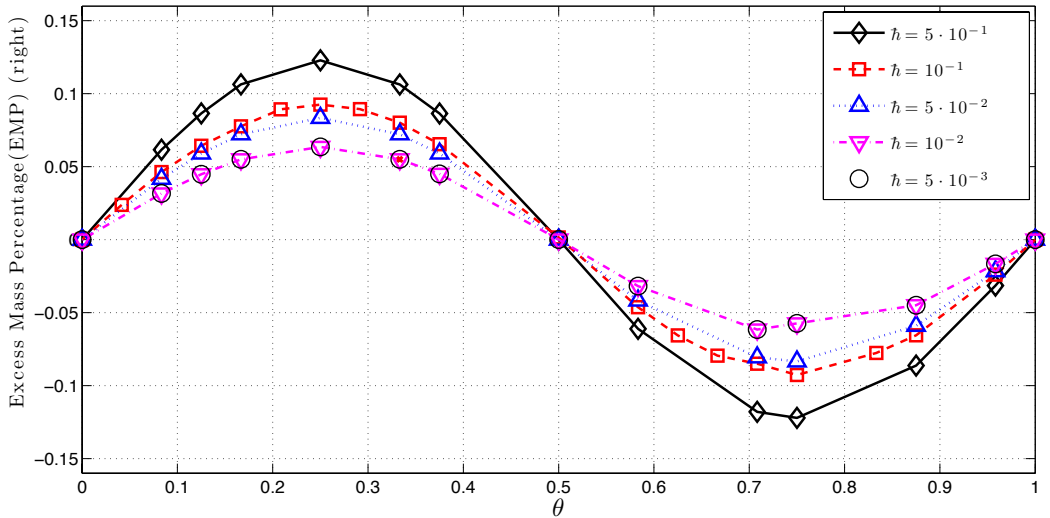

FIGURE 14. EMP distribution for various values of θ and $\hbar$.

6. Conclusions and Further Work

This work motivates the statement of the following

Conjecture. *Hypothesis 1 holds for non-interference problems (under appropriately regularity conditions for the initial data).*

A proof of this would provide a practical, elegant asymptotic tool for a family of problems that currently there exist none. A natural followup question would be to examine the generalizations of Hypothesis 1 for systems (i.e. on eigenvalue crossings).

As for interference problems, although we don't find Hypothesis 1 to hold, we do observe an apparent limiting behaviour; see Figure 14. It is natural to ask whether this is indeed a stable "quantum scattering operator", which depends only on the phase difference and has the apparent limiting amplitude of $\pm 5.5\%$.

It is also intriguing to ask if eq. (29) does indeed capture correctly the mass scattering and in general the observables of the problem for both interference and non-interference problems. It is not clear if it can be useful as a computational or asymptotic technique, but certainly one would like to eliminate it conclusively before giving up on trying to prove it.

As was mentioned earlier, the whole approach that we carried out here, makes sense for the investigation of the semiclassical limit of the Schrödinger-Poisson equation [35], which has essentially the same difficulties. There is a quantum equation, a multi-valued classical equation, and the question is if we can find a practical selection principle to connect the two. A lot of the machinery we use here for the linear problem can be extended to the Schrödinger-Poisson problem. So finally, the investigation of the quantum regularization of the Vlasov-Poisson equation with caustics is a very interesting possible next step.

Appendix A. Background on the Schrödinger equation and the Wigner transform

The Schrödinger equation (1) is well-posed on $L^2(\mathbb{R}^d)$ for real potentials V in Kato's class, i.e. if $V = V_1 + V_2$ and

$$(50) \qquad V_1 \in L^\infty, \quad V_2 \in L^p, \ p > \max\{2, \frac{d}{2}\}$$

or

$$(51) \qquad V_1 \in L^\infty, \ V_2 \in L^2_{loc}, \quad \text{and } \exists C > O \text{ such that } V_2 > -C(1 + |x|^2).$$

Practically all physically interesting cases are covered by these conditions – unlike the situation in classical mechanics. The Wigner transform (WT),

$$(52) \qquad W^\hbar : L^2(\mathbb{R}^d) \times L^2(\mathbb{R}^d) \to L^2(\mathbb{R}^{2d}) : f, g \mapsto W^\hbar[f, g] = \int e^{-2\pi i k y} f(x + \frac{\hbar y}{2}) \overline{g}(x - \frac{\hbar y}{2}) \, dy,$$

seen as a bilinear mapping is essentially unitary in L^2, in the sense that

$$\|W^\hbar[f, g]\|_{L^2(\mathbb{R}^{2d})} = \hbar^{-\frac{d}{2}} \|f\|_{L^2(\mathbb{R}^d)} \|g\|_{L^2(\mathbb{R}^d)}.$$

This allows the construction of an L^2 propagator for the Wigner equation out of the Schrödinger propagator [28]. We would like to interpret the WT as a phase-space probability density in the sense of classical statistical mechanics; it has e.g. the correct marginals as position and momentum density

$$(53) \qquad \int W^\hbar[f](x, k) \, dk = |f(x)|^2, \quad \int W^\hbar[f](x, k) \, dx = |\widehat{f}(x)|^2.$$

However this picture cannot be taken too literally, since the WT has negative values in general [11, 20]. In fact, it has been realized that when smoothed with an appropriately large kernel, the WT becomes non-negative. Skipping over some details, this can be seen as an equivalent reformulation of the Heisenberg uncertainty principle: one can get a valid (i.e. a priori non-negative) probability that a particle occupies a region in phase-space only if that region is large enough. This leads to the definition of the Husimi transform,

$$(54) \qquad H^\hbar[f](x, k) = \left(\frac{2}{\hbar}\right)^d e^{-\frac{2\pi}{\hbar}\left[|x|^2 + |k|^2\right]} * W^\hbar[f] \geqslant 0 \ \forall f \in L^2.$$

The Husimi transform is used to prove the positivity of the WM, since, as can be readily checked, $W^\hbar[u^\hbar]$ and $H^\hbar[u^\hbar]$ are close in weak sense as $\hbar \to 0$ [26].

The particular topology used for weak-$*$ convergence $W^\hbar[u^\hbar], H^\hbar[u^\hbar] \rightharpoonup W^0$ is built on the algebra of test functions $\mathcal{A}$, defined as

$$(55) \qquad \mathcal{A} = \{\phi \in C_0(\mathbb{R}^{2d}) \,|\, \int \sup_x |\mathcal{F}_{k \to K}[\phi(x, k)]| dK < \infty\}.$$

The main result for Wigner measures in smooth problems, precisely stated, is the following

Theorem A.1 (Wigner Measures for the linear Schrödinger equation [26, 18]). *Let the real valued potential V be in Kato's class, and assume there exists a $C > 0$ such that $V(x) \geqslant -C(1 + |x|^2)$, and that $V \in C^1(\mathbb{R})$. Assume moreover that the family of initial data $\{u_0^{\hbar_n}\}$, for a sequence $\lim\limits_{n\to\infty} \hbar_n = 0$, has the following properties*

- *($\hbar$-oscillation) If $F_\phi(R)$ is defined as*

$$F_\phi(R) = \limsup_{n\to\infty} \int\limits_{|k| \geqslant \frac{R}{\hbar_n}} |\widehat{\phi u_0^{\hbar_n}}|^2 \, dk,$$

  then, for all continuous, compactly supported ϕ

$$\lim_{R\to\infty} F_\phi(R) = 0.$$

- *(compactness) If $G(R)$ is defined by*

$$G(R) = \limsup_{n\to\infty} \int\limits_{|x| \geqslant R} |u_0^{\hbar_n}|^2 \, dx,$$

  then

$$\lim_{R\to\infty} G(R) = 0.$$

Then, for a semiclassical family of problems of the form (1), and any timescale $T > 0$, the following hold:

- *There exists a subsequence of the initial data, $u_0^{\hbar_{m_n}}$, so that their Wigner transform converges in $\mathcal{A}'$ weak-$*$ sense to a probability measure,*

$$\forall \phi \in \mathcal{A} \quad \lim_{n\to\infty} \langle W_0^{\hbar_{m_n}} - W_0^0, \phi \rangle = 0, \qquad W_0^0 \in \mathcal{M}_+^1(\mathbb{R}^{2d})$$

- *For $t \in [0,T]$, define $W^0(t)$ as the propagation of the initial Wigner measure W_0^0 under the Liouville equation (9). Then*

$$W^\hbar[u^{\hbar_n}(t)] = W^{\hbar_n}(t) \rightharpoonup W^0(t)$$

in $\mathcal{A}'$ weak-$*$ sense.

Appendix B. The Smoothed Wigner Transform

As was mentioned, sometimes flexibility in the calibration of the smoothing is required. Several approaches for the smoothing of the Wigner transform have been studied [11, 20], and there exist trade offs for the different choices and scalings of smoothing kernels. We use a Gaussian smoothing in what we call the Smoothed Wigner transform (SWT). This has the advantage that it leads to entire analytic functions of known order and type, thus making available a great toolbox of results for their asymptotic study [6].

The SWT was introduced in (25). Observe that

$$
\begin{aligned}
\widetilde{W}^\hbar[u](x,k) &= \left(\frac{2}{\hbar\sigma_x\sigma_k}\right)^d \int\limits_{x,k} e^{-\frac{2\pi}{\hbar}\left[\frac{|x-x'|^2}{\sigma_x^2} + \frac{|k-k'|^2}{\sigma_k^2}\right]} W^\hbar(x',k') \, dx' \, dk' = \\
&= \left(\frac{\sqrt{2}}{\sqrt{\hbar}\sigma_x}\right)^d \int\limits_y e^{-2\pi iky - \frac{\hbar\pi}{2}\sigma_k^2 y^2} \int\limits_{x'} e^{-\frac{2\pi}{\hbar}\frac{|x-x'|^2}{\sigma_x^2}} u(x' + \frac{y\hbar}{2})\overline{u}(x' - \frac{y\hbar}{2}) \, dx' \, dy,
\end{aligned}
$$

(56)

therefore only d convolutions are needed (i.e. in x), as the smoothing in k can be performed as part of the FFT.

To implement this transform numerically, we will use the FFT. First of all recall that

Lemma B.1. *For any function $f \in \mathcal{S}(\mathbb{R})$,*

$$\sum_{j\in\mathbb{Z}} f(jh)e^{-2\pi iknh} = \frac{1}{h} \sum_{j\in\mathbb{Z}} \widehat{f}(k + \frac{j}{h}).$$
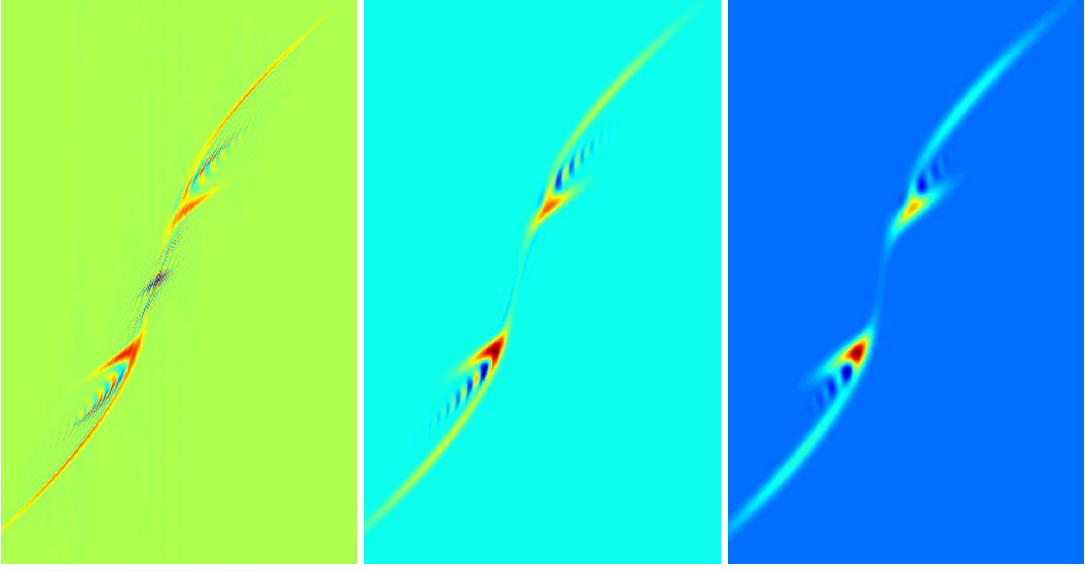
FIGURE 15. Smoothing of the Wigner transform. Left; the WT – dominant features correspond to oscillations that vanish in the limit. Middle; fine smoothing – the most spurious oscillations are gone, there is good resolution and some very negative values. Right; coarser smoothing, more appropriate for computational use – there are still non-negligible negative values, but the dominant features of the density are clearly positive while definition has not been overly smeared.

This is a direct corollary of the Poisson summation formula, and the starting point of any use of the FFT to approximate the Fourier transform of a continuous function. (The requirement $f \in \mathcal{S}(\mathbb{R})$ can be relaxed; the details along this direction are outside the scope of this work).

Similarly, we can create an appropriate version of the Poisson summation formula for the evaluation of the dy integral in (56) as an FFT:

Lemma B.2. *If $f \in \mathcal{S}(\mathbb{R})$, denote by*

$$S_{a,b}(X,y) = e^{-\frac{\pi}{2}\hbar\sigma_k^2 y^2} \int\limits_{x'} e^{-\frac{2\pi}{\hbar\sigma_x^2}(X-x')^2} f(x'+\hbar by)\overline{f}(x'-\hbar by)\,dx'.$$

Then

$$\sum_{j\in\mathbb{Z}} S_{a,b}(X,j)e^{-2\pi i 2Kaj} = \frac{\sigma_k^2}{b\sqrt{2}}\sum_{j\in\mathbb{Z}} \widetilde{W}[u](X,\frac{aK+j}{b}).$$

Observe that the integral $\int\limits_{x'} e^{-\frac{2\pi}{\hbar\sigma_x^2}(X-x')^2} f(x'+\hbar by)\overline{f}(x'-\hbar by)\,dx'$ only needs to be computed in a small interval in x' for each X because of the Gaussian localization.

APPENDIX C. SLICING IN TWO OF A WKB WAVEFUNCTION

A more singular non-interference problem example is given by the initial data

(57) $u_0(x) = a_0(x)e^{i\frac{S_0(x)}{\hbar}}, \quad a_0(x) = (1 + tanh(7(x+3))) \cdot (1 + tanh(7(-x+1))), \quad S_0(x) = \frac{-2}{3}|x|^{\frac{3}{2}}$

and

(58) $V(x) = 1 + (1 + \tanh(4(x+4)))(1 + \tanh(-4(x-4)))\frac{(-|x|+4)}{8}.$

The initial WM of this problem is a line supported measure. The concentration limit of $\rho^\hbar$ predicts that this measure would be "sliced" into two lines. We see clear qualitative agreement between $\rho^\hbar$ and $\widetilde{W}^\hbar$, see
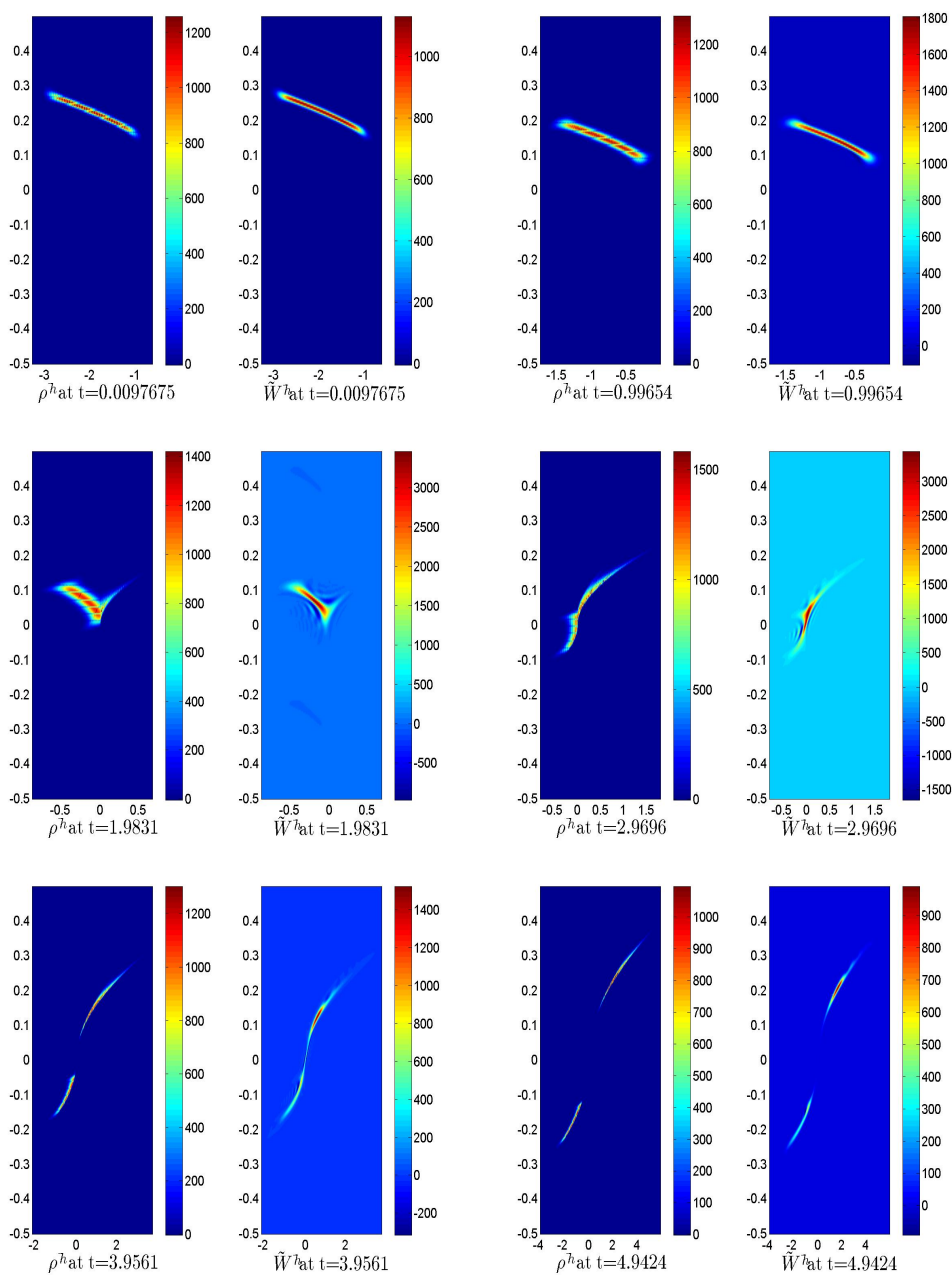
FIGURE 16. The quantum phase-space density $\widetilde{W}^{\hbar}(t)$ versus its proposed semiclassical approximation $\rho^{\hbar}(t)$, for the data of eq. (57), $\hbar = 10^{-2}$ and various times before, during, and after interaction with the singularity.

Figure 16. The quantum observables (46) (including mass scattered to the left / right) are within around 4% of their semiclassical prediction. Overall it seems that quantitative convergence as $\hbar \to 0$ is taking place, albeit somewhat more slowly for this type of initial data than for the data of eq. (45).

The numerical solution for $\rho^{\hbar}$ (i.e. of the Liouville equation (27)) is more challenging for this problem, than for the initial data of (45) because of the singularity of the flow.

References

[1] G. Akrivis, Ch. Makridakis, & R. H. Nochetto, *A posteriori error estimates for the Crank-Nicolson method for parabolic equations*, Math. Comp. **75** (2006) pp. 511–531.

[2] L. Ambrosio & A. Figalli, *Almost everywhere well-posedness of continuity equations with measure initial data*, C. R. Math. Acad. Sci. Paris **348** 56 (2010) pp. 249–252.

[3] L. Ambrosio, G. Friesecke & J. Giannoulis, *Passage from Quantum to Classical Molecular Dynamics in the Presence of Coulomb Interactions*, Comm. Partial Differential Equations **35** (2010) pp. 1490–1515.

[4] L. Ambrosio, A. Figalli, G. Friesecke, J. Giannoulis & T. Paul, *Semiclassical limit of quantum dynamics with rough potentials and well posedness of transport equations with measure initial data*, Comm. Pure Appl. Math. **64** 9 (2011) pp. 1199–1242.

[5] A. Athanassoulis & T. Paul, *On the selection of the classical limit for potentials with BV derivatives*, J. Dynam. Differential Equations **25** 1 (2013) pp. 33–47.

[6] A. Athanassoulis, N.J. Mauser & T. Paul, *Coarse-scale representations and smoothed Wigner transforms*, J. Math. Pures Appl. **91** 3 (2009) pp. 296–338.

[7] A. Bamberger, B. Engquist, L. Halpern & P. Joly, *Higher order paraxial wave equation approximations in heterogeneous media*, SIAM J. Appl. Math. **48** 1 (1988) pp. 129 – 154.

[8] W. Bao, S. Jin, & P.A. Markowich *Numerical Study of Time-Splitting Spectral Discretizations of Nonlinear Schrdinger Equations in the Semiclassical Regimes*, SIAM J. Sci. Comput. **25** 1 (2003) pp. 27–64.

[9] F. Bouchut, *Renormalized Solutions to the Vlasov Equation with Coefficients of Bounded Variation*, Arch. Ration. Mech. Anal. **157** 1 (2001) pp. 75–90.

[10] R. Carles, C. Fermanian-Kammerer, N.J. Mauser & H.P. Stimming, *On the time evolution of Wigner measures for Schrodinger equations*, Commun. Pure Appl. Anal. **8** 2 (2009) pp. 559–585.

[11] L. Cohen, *Time frequency distributions - a review*, Proc. IEEE, **77** 7 (1989) pp. 941–981.

[12] M. Combescure & D. Robert, *Coherent States and Applications in Mathematical Physics*, Springer, 2012.

[13] M. de Hoop, G. Hörmann & M. Oberguggenberger, *Evolution systems for paraxial wave equations of Schrödinger-type with non-smooth coefficients*, J. Differential Equations **245** 6 (2008) pp. 1413–1432.

[14] W. Dörfler, *A time-and space-adaptive algorithm for the linear time-dependent Schrödinger equation*, Numer. Math. **73** (1996) pp. 419–448.

[15] L. C. Evans, *Partial Differential Equations*, 2nd edition, American Mathematical Society, 2010.

[16] C. Fermanian Kammerer, P. Gérard *A Landau-Zener Formula for Non-Degenerated Involutive Codimension 3 Crossings*, Ann. Henri Poincaré **4** 3 (2003) pp. 513–552.

[17] C. Fermanian-Kammerer, P. Gérard & C. Lasser, *Wigner Measure Propagation and Conical Singularity for General Initial Data*, Arch. Ration. Mech. Anal. **209** 1 (2013) pp. 209–236.

[18] P. Gérard, P. Markowich, N. J. Mauser & F. Poupaud, *Homogenization limits and Wigner transforms*, Comm. Pure Appl. Math. **50** 4 (1997) pp. 323–379.

[19] L. Harris, J. Lukkarinen, S. Teufel & F. Theil, *Energy Transport by Acoustic Modes of Harmonic Lattices*, (2008) SIAM J. Math. Anal., **40** 4 pp. 1392–1418.

[20] F. Hlawatsch & G. F. Boudreaux-Bartels, *Linear and quadratic time-frequency signal representations*, (1992) IEEE Signal Proc. Mag. **9** 2 pp. 21–67.

[21] S. Jin P.A. Markowich & C. Sparber, *Mathematical and Computational methods for semiclassical Schrödinger equations*, Acta Numer. **20** (2011) pp. 121–209.

[22] Th. Katsaounis & I. Kyza, *A posteriori error control and adaptivity for Crank-Nicolson finite element approximations for the linear Schrdinger equation*, to appear in Numer. Math.

[23] C. Lasser & S. Teufel, *Propagation through conical crossings: An asymptotic semigroup*, Comm. Pure Appl. Math. **58** 9 (2005) pp. 1188–1230.

[24] M. Lax, W. H. Louisell & W. B. McKnight, *From Maxwell to paraxial wave optics*, Phys. Rev. A **11** 4 (1975) pp. 1365–1370.

[25] S. Leung, J. Qian & S. Osher, *A level set method for three-dimensional paraxial geometrical optics with multiple point sources*, Commun. Math. Sci. **2** 4 (2004) pp. 643–672.

[26] P.L. Lions & T. Paul, *Sur les mesures de Wigner*, Rev. Mat. Iberoam. **9** 3 (1993) pp. 553–618.

[27] Ch. Makridakis, R.H. Nochetto, *Elliptic reconstruction and a posteriori error estimates for parabolic problems*, SIAM J. Numer. Anal. **41** (2003) pp. 1585–1594.

[28] P.A. Markowich & H.Neunzert, *On the equivalence of the Schrdinger and the quantum Liouville equations*, Math. Methods Appl. Sci. (1989) **11** 4 pp. 459–469.

[29] A.A.M. Marte & S. Stenholm, *Paraxial light and atom optics: the optical Schrödinger equation and beyond*, Phys. Rev. A **56** 4 (1997) pp. 2940–2953.

[30] A. Mielke, *Macroscopic behavior of microscopic oscillations in harmonic lattices via Wigner- Husimi transforms*, Arch. Ration. Mech. Anal. **181** (2006) pp. 401–448.

[31] L. Miller, *Refraction of high-frequency waves density by sharp interfaces and semiclassical measures at the boundary*, J. Math. Pures Appl. **79** 3 (2000) pp. 227–269.

[32] L. Ryzhik , G. Papanicolaou & J. B. Keller, *Transport equations for elastic and other waves in random media*, Wave Motion **24** (1996) p. 327–370

[33] C. Sparber, P. Markowich & N. J. Mauser, *Wigner Functions versus WKB-Methods in Multivalued Geometrical Optics*, Asymptot. Anal. **33** 2 (2003) pp. 153–187.

[34] S. Teufel, *Adiabatic Perturbation Theory in Quantum Dynamics*, Springer, 2003.

[35] P. Zhang, Y. Zheng & N.J. Mauser, *The limit from the Schrödinger-Poisson to the Vlasov-Poisson equations with general data in one dimension*, Comm. Pure Appl. Math. **55** 5 (2002) pp. 582–632.

(A. Athanassoulis) DEPT. OF MATHEMATICS, UNIVERSITY OF LEICESTER, UK
E-mail address: agis.athanasoulis@le.ac.uk

(Th. Katsaounis) DEPT. OF MATH. AND APPLIED MATH. , UNIVERSITY OF CRETE, & INSTITUTE OF APPLIED AND COMPU-
TATIONAL MATHEMATICS–FORTH, NIKOLAOU PLASTIRA 100, VASSILIKA VOUTON, HERAKLION-CRETE GREECE
E-mail address: thodoros@tem.uoc.gr

(I. Kyza) DIVISION OF MATHEMATICS, UNIVERSITY OF DUNDEE, DUNDEE, DD1 4HN, SCOTLAND, UK & INSTITUTE OF APPLIED
AND COMPUTATIONAL MATHEMATICS–FORTH, NIKOLAOU PLASTIRA 100, VASSILIKA VOUTON, HERAKLION-CRETE, GREECE.
E-mail address: ikyza@maths.dundee.ac.uk